

Synthesis, Electrochemistry and Chemical Reactivity of Heteroleptic Indium 2-Amidophenolates

By

Grace Amelia Leech

A thesis submitted to the

Department of Chemistry and Biochemistry

Mount Allison University

In partial fulfillment of the requirements for the

Bachelor of Science degree with Honours

April 2023

Thesis Committee

Supervisor

Dr. Glen Briand
Professor of Chemistry

Reviewer

Dr. Sarah McOnie
Assistant Professor of Chemistry

Table of Contents

Thesis Committee	1
Acknowledgments	4
List of Tables, Figures, and Schemes	6
List of Spectra in Appendix	8
Glossary of Abbreviations and Symbols	10
Abstract	11
1. Introduction	12
1.1 Green Chemistry.....	12
1.2 Catalysis.....	15
1.3 Indium.....	17
1.4 Redox Active Ligands.....	17
1.5 Current Study.....	21
2. Experimental	22
2.1 General Methods and Considerations.....	22
2.2 Synthesis of (NCN)Br (1).....	22
2.3 Synthesis of (NCN)InMe ₂ (2).....	23
2.4 Synthesis of H ₂ (NO) (3).....	23
2.5 Synthesis of (NC)InMe ₂ (4).....	24
2.6 Synthesis of (NCN)InCl ₂ (5).....	24
2.7 Synthesis of (Me)In(NO) (6).....	25
2.8 Synthesis of (NCN)In(HNO) ₂ (7).....	25
2.9 Synthesis of (NCN)In(NO) (8).....	26
2.10 Synthesis of (NCN)InI ₂ (9).....	27
2.11 Attempted synthesis of (NCN)In(NO) ₂ (12).....	27
2.12 Cyclic voltammetry.....	28
2.13 Computational methods (NCN)In(NO) (8).....	29
2.14 X-ray Crystallography.....	29
3. Results and Discussion	31
3.1 Synthesis of H ₂ (NO) (3).....	31
3.2 Synthesis of (Me)In(NO) (6).....	32
3.3 Synthesis of (NCN)In(HNO) ₂ (7).....	33
3.4 X-ray crystal structure of (NCN)In(HNO) ₂ (7).....	34
3.5 Synthesis of (NCN)In(NO) (8).....	35
3.6 X-ray crystal structure of (NCN)In(NO) (8).....	37
3.7 Reaction of (NCN)In(NO) (8) with Diiodine.....	38

3.8	X-ray crystal structure of (NCN)InI ₂ (9).....	40
3.9	Computational studies of (NCN)In(NO) (8).....	41
3.10	Reaction of (NCN)In(NO) (8) with Dioxygen.....	43
3.11	Cyclic Voltammetry of (NCN)In(NO) (8).....	44
4.	Conclusion	48
5.	Future Directions	48
6.	References	49
7.	Appendix	54

Acknowledgments

I would like to begin by expressing my appreciation to Dr. Briand, not only for his advice and guidance but also his patience and encouragement throughout the research conducted to complete my thesis. Dr. Briand took me under his wing in the summer of 2021 and I have enjoyed working alongside him since. It is thanks to him, that this work has been possible and that I am the researcher I am today.

Second, I would like to extend my thank you's to various professors within the department. Beginning with Dr. McOnie, my second reader, and an important member of my honours committee. Dr. McOnie brought a new point of view upon her recent arrival to Mount Allison University and has helped me in finding the appreciation I have for chemistry today. Next, I would like to thank the late Dr Steve Westcott. Dr Westcott was an extraordinary professor and a key member of the chemistry and biochemistry department throughout his time at Mount Allison. He motivated his students to take the initiative on one's education and continuously gave countless opportunities to find one's passion. Dr Westcott, I will never forget the nickname you gave me, and I will do what I can to continue being a rockstar. Thank you for helping me gain the confidence I have today both as a person and as a chemist.

My thank you's extend to the Metal Heads that I have been lucky to call my lab mates, Alex, Padma, John and Maddie. Thanks to their company, the 3 hours plus stir times seemed to always find a way to fly by. A special thank you goes to Padma for her help with the theoretical calculations. I express gratitude to Dr. Jason Masuda and Tanner George at Saint Mary's University for the X-ray crystallography analysis and Brian Maclean at Saint Francis Xavier University for the cyclic voltammetry analysis.

This research could not have been possible without the training provided by Phil Cormier, Eva Zhou, Susan Wheaton and Danny Durant. It is thanks to these technicians that I felt safe and well equipped to perform my research over the past years. A final thank you goes out to the lifelong friends I have made over the past four years as well as my family for encouraging me to realize the potential I hold. With good company comes lifelong memories. I thank you all for being apart of something so special to me & for helping shape me into the researcher I am today.

Kind regards,

Grace Amelia Leech

List of Tables, Figures & Schemes

Figure 1: The Twelve Principles of Green Chemistry.

Figure 2: Synthesis of Sertraline.

Figure 3: The Catalytic Cycle of Wilkinson's Catalyst.

Figure 4: Two sequential one-electron redox processes performed on the amidophenolate ligand.

Figure 5: Redox-active amidophenolate ligands involved in the catalytic disproportionation of diphenyl hydrazine.

Figure 6: Target compounds of the current study: (Me)In(NO) (**6**) and (NCN)In(NO) (**8**) where NCN = {2,6-bis[(dimethylamino)methyl]phenyl}.

Figure 7: X-ray crystal structure of (NCN)In(HNO)₂. Hydrogen atoms are removed for clarity.

Figure 8: X-ray crystal structure of (NCN)In(NO). Hydrogen atoms are removed for clarity.

Figure 9: X-ray crystal structure of (NCN)InI₂. Hydrogen atoms are removed for clarity.

Figure 10: Geometry optimized structures of (NCN)In(NO) (**8**), (NCN)InI₂ (**9**), neutral iminobenzosemiquinone (**11**) and [(NCN)InI(NO)]' (**10**). Hydrogen atoms are omitted for clarity.

Figure 11: HOMO front view (left) and side view (right) of **8**.

Figure 12: LUMO front view (left) and side view (right) of **8**.

Figure 13: Cyclic voltammogram (0.01 V, 0.05 V, 0.10 V, 1 mM) of **8** in CH₃CN, 0.1 M [Bu₄][NPF₆], 23°C in acetonitrile under a dinitrogen atmosphere.

Figure 14: Chemical structures of (NCN)In(NO) (**8**) and its solvated form (NCN)In(NO)(MeCN) (**8**•MeCN).

Table 1: Crystallographic data for Compounds **7-9**.

Scheme 1: Redox activity of the amidophenolate ligand (NO) (**3**).

Scheme 2: Reaction scheme for the synthesis of H₂(NO) (**3**).

Scheme 3: Reaction scheme for the synthesis of (Me)In(NO) (**6**).

Scheme 4: Reaction scheme for the synthesis of (NCN)In(HNO)₂ (**7**).

Scheme 5: Reaction scheme for the synthesis of (NCN)In(NO) (**8**).

Scheme 6: The expected synthetic route of the oxidation of (NCN)In(NO) with diiodine.

Scheme 7: Chemical oxidation of **8** with 0.5 equivalents of I₂ resulting in the formation of (NCN)InI₂ (**9**).

Scheme 8: Chemical oxidation of **8** with 1 equivalent of I₂ resulting in the formation of (NCN)InI₂ (**9**).

Scheme 9: Chemical oxidation of **8** with O₂ resulting in the potential formation of (NCN)In(NO)₂ (**10**).

Scheme 10: Solvation of **8** with MeCN resulting in the formation of **8**•MeCN.

List of Spectra in Appendix

Figure A.1: ^1H NMR spectrum of $(\text{NCN})\text{Br}$ (**1**) in CDCl_3 .

Figure A.2: ^1H NMR spectrum of $(\text{NCN})\text{InMe}_2$ (**2**) in DMSO.

Figure A.3: ^1H NMR spectrum of $\text{H}_2(\text{NO})$ (**3**) in CDCl_3 .

Figure A.4: ^1H NMR spectrum of $(\text{NC})\text{InMe}_2$ (**4**) in CDCl_3 .

Figure A.5: ^1H NMR spectrum of $(\text{NCN})\text{InCl}_2$ (**5**) in CDCl_3 .

Figure A.6: FT-IR spectrum of $(\text{NCN})\text{InCl}_2$ (**5**).

Figure A.7: ^1H NMR spectrum of $(\text{NCN})\text{In}(\text{HNO})_2$ (**7**) in CDCl_3 .

Figure A.8: $^{13}\text{C}\{^1\text{H}\}$ NMR spectrum of $(\text{NCN})\text{In}(\text{HNO})_2$ (**7**) in CDCl_3 .

Figure A.9: FT-IR spectrum of $(\text{NCN})\text{In}(\text{HNO})_2$ (**7**).

Figure A.10: ^1H NMR spectrum of $(\text{NCN})\text{In}(\text{NO})$ (**8**) in CDCl_3 .

Figure A.11: $^{13}\text{C}\{^1\text{H}\}$ NMR spectrum of $(\text{NCN})\text{In}(\text{NO})$ (**8**) in CDCl_3 .

Figure A.12: FT-IR spectrum of $(\text{NCN})\text{In}(\text{NO})$ (**8**).

Figure A.13: ^1H NMR spectrum of 0.5 equivalents of I_2 added to $(\text{NCN})\text{In}(\text{NO})$ in CDCl_3 .

Figure A.14: ^1H NMR spectrum of 1 equivalent of I_2 added to $(\text{NCN})\text{In}(\text{NO})$ in CDCl_3 .

Figure A.15: ^1H NMR spectrum of 1.5 equivalents of I_2 added to $(\text{NCN})\text{In}(\text{NO})$ in CDCl_3 .

Figure A.16: ^1H NMR spectrum of $(\text{Me})\text{In}(\text{NO})$ (**6**) in CDCl_3 .

Figure A.17: ^1H NMR spectrum of $(\text{NCN})\text{InI}_2$ (**9**) in CDCl_3 .

Figure A.18: $^{13}\text{C}\{^1\text{H}\}$ NMR spectrum of $(\text{NCN})\text{InI}_2$ (**9**) in CDCl_3 .

Figure A.19: FT-IR spectrum of $(\text{NCN})\text{InI}_2$ (**9**).

Figure A.20: ^1H NMR spectrum of reacting **8** with O_2 in CDCl_3 .

Figure A.21: $^{13}\text{C}\{^1\text{H}\}$ NMR spectrum of reacting **8** with O_2 in CDCl_3 .

Figure A.22: FT-IR spectrum of reacting **8** with O_2 .

Glossary of Abbreviations and Symbols

Symbol	Definition
Me	Methyl (CH ₃)
NCN	Pincer Ligand [C ₆ H ₃ -2,6-(CH ₂ NMe ₂) ₂]
THF	Tetrahydrofuran
Et ₂ O	Diethyl Ether
CDCl ₃	Deuterated Chloroform
M	Molarity (mol/L)
mL	Millitre
mmol	Millimole
NMR	Nuclear Magnetic Resonance
ppm	Parts per million
J	Coupling Constant
d	Doublet
t	Triplet
IR	Infrared Spectroscopy
tBu	tert-butyl
py	Pyridine
h	Hour
min	Minute

Abstract

Green chemistry aims to design chemical products and processes that reduce the amount of waste production within the chemical industry. Catalysis is a primary tenet of the Twelve Principles of Green Chemistry as it circumvents the need for stoichiometric amounts of reactants. The use of main group metals is a viable alternative to expensive and toxic precious metals required to facilitate chemical transformations for the pharmaceutical and fine chemical industries. Specifically, indium-based compounds possess numerous advantageous characteristics such as its low toxicity, low cost and its functional group tolerance. Amidophenolate ligands are ubiquitous in organometallic chemistry and may be employed as non-innocent redox-active ligands. The aim of this research is to investigate the use of redox active non-innocent amidophenolate ligands for the synthesis, electrochemistry, and chemical reactivity of indium complexes to ultimately enlist them as redox active materials.

1. Introduction

1.1 Green Chemistry

The concept of Green Chemistry began in the early 1990's and has since been an emerging field of research. Its goal includes working at the molecular level in order to achieve sustainability.¹ The definition of Green Chemistry is the “design of chemical products and processes to reduce or eliminate the use and generation of hazardous substances”.¹ Green Chemistry seeks to synthesize chemicals that are “benign by design”, which means to reduce overall risk by designing chemicals and processes that are intrinsically less harmful than those of traditional methods.² In order to be considered green, there are three components of a reaction that must be optimized, notably the solvent, reagent/catalyst and energy consumption.³

The traditional practice in reducing health and environmental risks that are associated with chemical reactions is the design of rules regarding circumstantial factors, notably the use, handling and disposal of said chemicals.⁴ Alternatively, Green Chemistry focuses on reducing risk factors by minimizing the use of hazardous materials. Examples of this include the design or selection of chemicals that have reduced toxicity and are not susceptible to undesired secondary reactivity. The ability to manifest hazard is reduced, meaning there is less risk at hand.⁴

The three overarching themes within the field of Green Chemistry are to design across all stages of the chemical life cycle, to design the inherent nature of the chemical products and reactions to reduce intrinsic hazard, and to work as a cohesive system of twelve principles.¹ The Twelve Principles of Green Chemistry were first introduced in the late 1990's by Paul Anastas and John Warner (**Figure 1**). These served as a guiding framework in the design of new reactions and products, as well as sustainability. The Principles as a whole apply to various aspects of the process life-cycle and address safety and efficiency of transformation, raw materials used, toxicity of

reagents and products used through reactions.¹ When designing a Green Chemistry process, it is nearly impossible to meet the demands of all Twelve Principles simultaneously, however, as many principles as possible are incorporated throughout crucial stages of synthetic processes.³

The Twelve Principles of Green Chemistry	
I. Prevention	VII. Use of Renewable Feedstocks
II. Atom Economy	VIII. Reduce Derivatives
III. Less Hazardous Chemical Synthesis	XI. Catalysis
IV. Design of Safer Chemicals	X. Design for Degradation
V. Safer Solvents and Auxiliaries	XI. Real-Time Analysis for Pollution Prevention
VI. Design for Energy Efficiency	XII. Inherently Safer Chemistry for Accident Prevention

Figure 1: The Twelve Principles of Green Chemistry.

The development of new pharmaceutical products through organic synthesis has continued to be revolutionary for medical care by enabling sizable reductions in hospitalization sufferings and deaths. However, this has come with significant environmental impact such as pharmaceuticals passing through our bodies into the waterways. This is being alleviated with the recent increasing emphasis on Green Chemistry, as pharmaceutical chemists have directed their focus onto minimizing the environmental impact of their processes.⁵

The pharmaceutical industry's efforts to reduce the amount of waste in existing synthetic routes features the success of The Twelve Principles of Green Chemistry. An ever-evolving method to combat this issue is the use/selection of green solvents, otherwise known as environmentally friendly solvents.⁵ An example of this would be the synthesis of Sertraline.

Sertraline is a well-known anti-depressant agent originally launched by Pfizer in the early 1990's. The initial procedure utilized four steps to construct the skeleton of the racemic tetralone. The original synthesis also included a Friedel Crafts acylation that required excess AlCl_3 , which was carried out in the hazardous solvent, carbon disulfide. The final step of the original synthesis involved the use of a chiral salt. Significant resources were required in order to carry the unwanted stereoisomer throughout the synthetic series.⁵ There are various ways in which we could make this synthesis more green such as taking a shorter route to obtain the initial skeleton of the racemic tetralone and using an alternative green solvent in the Friedel Crafts acylation. The original synthesis was not considered a green process as near half of the targeted product was unused diastereomer that was not recycled.⁵

The formation of the imine in the Sertraline synthesis could reach up to 95% completion by replacing the solvent tetrahydrofuran (THF) with ethanol, which is classified as a green solvent (**Figure 2**). As a result of low solubility, the equilibrium of the condensation was then conveyed towards the imine, which precipitated from the reaction mixture. Due to this, TiCl_4 was no longer necessary for the imine formation, thus afforded an improved procedure that circumvented the difficult separation of the titanium waste and its expensive disposal.⁵ Rather than accepting waste production and disposal as inescapable, Green Chemistry attempts to find new cleaner technologies that are economically competitive. Green Chemistry is used for pollution prevention using careful design, to benefit the environment.⁶

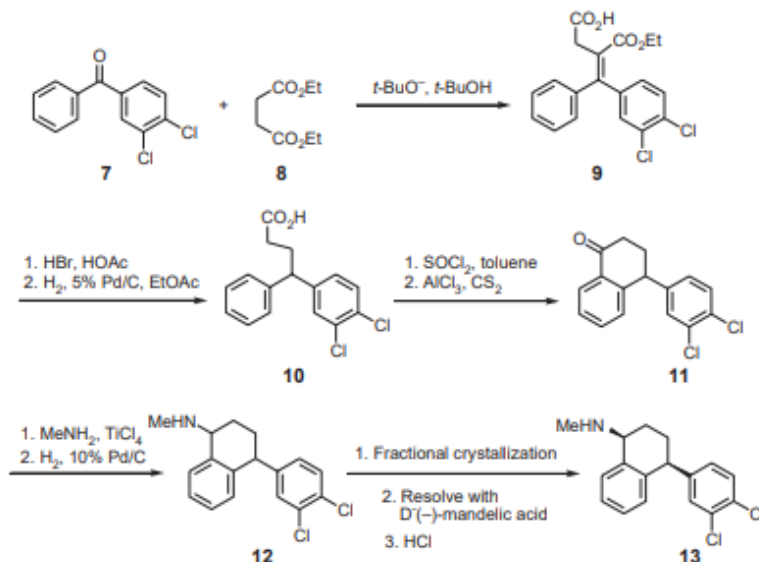


Figure 2: Synthesis of Sertraline.⁵

1.2 Catalysis

Catalysis is one of the Twelve Principles of Green Chemistry meaning it is a fundamental pillar in this area of research. The synthesis of novel catalysts and catalytic systems are important in achieving environmental protection as well as an economic benefit.⁶ Catalysis has applications in fields ranging from pharmaceuticals to polymers to petroleum processing. Up to 90% of all industrial processes employ catalysis.⁶

Waste production in industrial processes is often connected to the traditional use of stoichiometric amounts of reagents. A substantial way to improve the efficiency of the synthetic toolbox is by switching stoichiometric methodologies to catalytic processes. There are many ways in which catalysis can improve the productivity of a reaction, such as lowering the necessary energy input, avoiding the use of stoichiometric amount of reagents and increasing product selectivity.¹ The Twelve Principles of Green Chemistry highlight catalysis as one of the most important steps to implementing Green Chemistry as it offers many advantages such as lower

energy requirements, decreased use of processing and separation agents and less use of particularly toxic materials.⁶

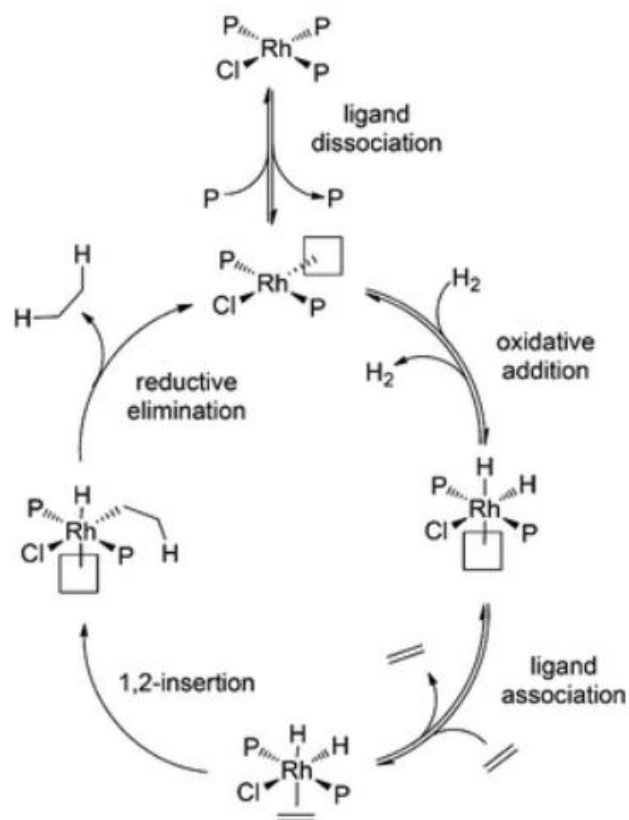


Figure 3: The Catalytic Cycle of Wilkinson's Catalyst.⁷

Wilkinson's catalyst is an example of an inorganic catalyst precursor containing a redox-active metal centre, Rhodium, where it may adopt a change in oxidation state.⁸ Wilkinson's catalyst is commonly used for its homogenous catalytic hydrogenation in the reduction of alkenes (**Figure 3**).⁹ The hydrogenation of an alkene is facilitated when the organic reagent attaches itself to the metal. This occurs due to the organic group being primarily susceptible to the nucleophilic attack. The targeted product is then produced through the reductive elimination of the organic group. Precious metals such as second and third row transition metals are often used in these types

of organometallic catalysts as they possess the ability to undergo the two-electron oxidation state changes that are crucial for the oxidative addition and reductive elimination steps of the proposed cycle.⁹

1.3 Indium

Indium is a trivalent, heavy main group metal. Although, indium does not possess any redox activity on its own, through the incorporation of redox active ligands it is possible to convey redox activity on indium-based compounds.¹⁰ There are multiple properties of indium that make it a desirable metal for use in Green chemical processes such as its low toxicity, low cost and its functional group tolerance.¹¹ Indium is known for its potential use as Lewis acid catalysts in aqueous solutions. Aprotic organic solvents are a necessity when considering water sensitive processes which makes indium compounds beneficial in this area. This being said, there are many factors that make these solvents harmful for the environment such as flammability, volatility and its risk of environmental release.¹²

Indium is a group 13, fifth row element and can form bonds using its three valence electrons that are found in the 5s and 5p orbitals. Indium is typically found in its most stable oxidation state of +3. Indium(III), in comparison to other effective organometallic centres such as boron(III), is found to be less reactive and a known soft Lewis acid.^{13,14} Due to its high chemo-selectivity, however, it has a high tolerance for organic functional groups such as aldehydes, ketones and amines.

1.4 Redox Active Ligands

A redox-active ligand is defined as a ligand that may undergo reversible reduction or oxidation. The two major types of reactivity where the redox non-innocent ligand is involved in are the following: the redox active ligand participates in the catalytic cycle by either accepting or

donating electrons and the redox active ligand participates in the formation or breaking of substrate covalent bonds.¹⁵ Throughout the redox process it is the oxidation state of the ligand that is altered while the oxidation state of the coordinated metal remains unchanged. Often, this can be the cause of some uncertainty while assigning oxidation states to the ligand and the metal.^{16,17} Since, redox-active ligands can accept or lose one or more electrons reversibly without the loss of coordination to the metal, a redox-active ligand bonded to a main group metal, such as indium, is then able to reduce or oxidize a substrate that is coordinated to the metal (**Figure 4**).¹⁸

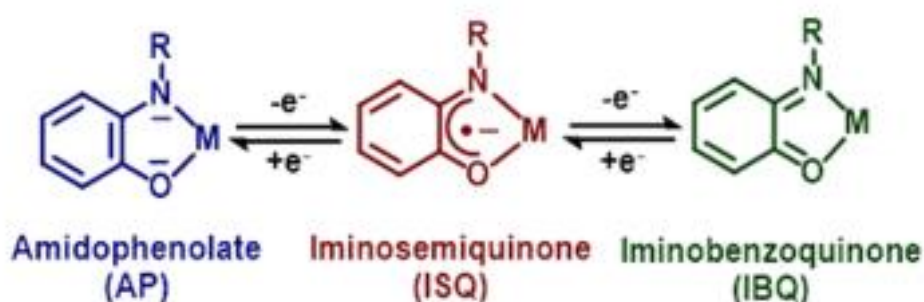
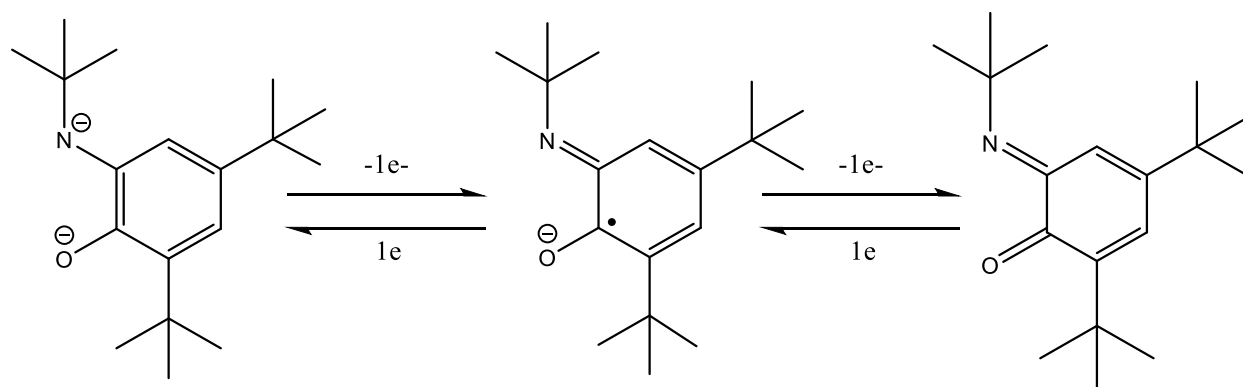


Figure 4: Two sequential one-electron redox processes performed on the amidophenolate ligand.¹⁹

A common approach to making redox active compounds involves attaching a redox-active non-innocent ligand to the metal centre. The term “non-innocent” refers to an inexplicit oxidation state of the metal complex that includes redox-active ligands.²⁰ There are various ways in which the incorporation of a redox active ligand can alter the reactivity of the metal complex. These include affecting the Lewis acidity, acting as electron reservoirs, participating in radical redox chemistry and forming ligand radicals.²¹ It is advantageous when redox-active ligands act as electron reservoirs in the sense that the oxidation state on the metal centre is unchanged while the ligand participates in the electron transfer reactions. This prevents the metal centre from adopting unfavourable oxidation states.²²

An example of a redox active non innocent ligand is an amidophenolate ligand, that coordinates to the indium metal centre to help convey redox activity and produce redox active compounds. Amidophenolate ligands are redox active when fully deprotonated and are described as dianionic ligand (**Scheme 1**). The oxidation states of these non innocent ligands are altered through redox processes whilst the oxidation state of the coordinated metal remains the same.



Scheme 1: Redox activity of the amidophenolate ligand (NO) (**3**).

Indium(III) complexes have recently been explored for their use in redox-active ligand catalytic transformations. Since 2000, the use of bulky amidophenolate ligands has increased immensely due to the work of Wieghardt.¹⁹ These ligands have recently been significantly popularized due to the easy access of two sequential one-electron redox processes that are found affordable on the ligand backbone (**Figure 4**).¹⁹ With such ligands, a large amount of the electron trafficking occurs directly on the ligand rather than on the metal centre.¹⁶ Research performed by Heyduk et al. (**Figure 5**) combined amido bis(phenolate) ligands with Zr(IV) (compound **13**) in order to achieve a formal oxidative addition of Cl₂ resulting in complex **14**. With this, they were able to perform oxidative addition with a d⁰ metal complex.¹⁶

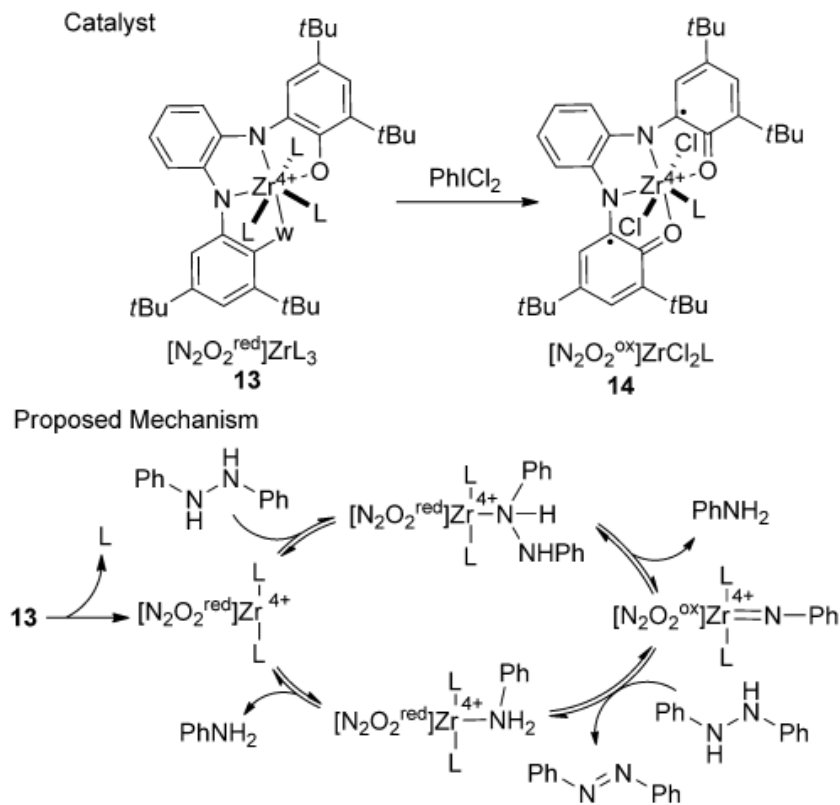


Figure 5: Redox-active amidophenolate ligands involved in the catalytic disproportionation of diphenyl hydrazine.¹⁶

While numerous redox-active ligands have been studied with various main group metals, the following work focuses on the redox processes involving amidophenolate (NO) ligand interactions with indium metal.

1.5 Current Study

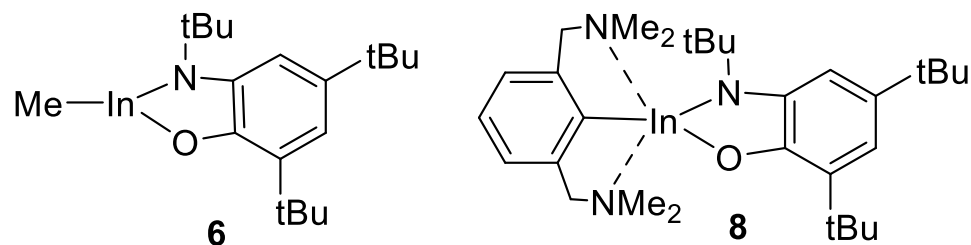


Figure 6: Target compounds of the current study: (Me)In(NO) (**6**) and (NCN)In(NO) (**8**) where NCN = {2,6-bis[(dimethylamino)methyl]phenyl}.

The goal of the current study is to synthesize and characterize redox active indium complexes using amidophenolate ligands (**Figure 6**). Redox activity is conveyed to the compound through the redox-active amidophenolate ligand.²³ The properties of the indium complexes will be modified by substituting the organic group of RIn(NO), where R = NCN (**1**) or R = Me (**2**). Both target compounds will be characterized using ¹H and ¹³C{¹H} NMR spectroscopy, melting point, elemental analysis and FT-IR spectroscopy. The structural motifs of the isolated compounds will be confirmed using X-ray crystallography. Their electrochemical properties will be analyzed using cyclic voltammetry and their chemical reactivity with oxidizing agents diiodine, diphenyl sulfide and dioxygen will be tested. Finally, computation studies will be used to rationalize the observations from these studies.

2. Experimental

2.1 General Methods and Considerations

2.1.1 Instrumentation

Air and moisture sensitive reactions were performed under a dinitrogen atmosphere using standard Schlenk techniques and an Innovative Technology glovebox unless otherwise stated. ^1H and $^{13}\text{C}\{^1\text{H}\}$ NMR spectra were collected using a Varian Mercury 200 MHz+ spectrometer (200 and 50.3 MHz, respectively) at 25°C. FT-IR spectra were recorded using a Thermo Nicolet diamond ATR spectrometer. Melting points were determined using an Electrothermal MEL-TEMP apparatus. Single-crystal X-ray crystallography was performed by Dr. Jason Masuda at Saint Mary's University. Elemental analysis was performed by Guelph Chemical Laboratories Inc.

2.1.2 Reagents

Anhydrous tetrahydrofuran (THF) ($\geq 99.9\%$ inhibitor-free), anhydrous diethyl ether ($\geq 99.7\%$), anhydrous toluene (99.8%), anhydrous hexane (95%), anhydrous pentane ($\geq 99\%$), and anhydrous acetonitrile (99.8%) were purchased from Sigma Aldrich and dried over molecular sieves. Indium (III) chloride anhydrous powder (98%), *n*-BuLi (1.6 M in hexanes), 3,5-di-*tert*-butylcatechol (98%) and *tert*-butylamine (98%) were obtained from Sigma Aldrich. Trimethylindium was obtained from Strem Chemicals. Ethyl alcohol anhydrous (99%) was obtained from Greenfield Global. $\text{C}_6\text{H}_3\text{Br}-2,6-(\text{CH}_2\text{Br})_2$ ²⁴ was prepared as reported previously.

2.2 Synthesis of (NCN)Br (1)

$\text{C}_6\text{H}_3\text{Br}-2,6-(\text{CH}_2\text{Br})_2$ (18.77 g, 54.75 mmol) and Me_2NH (234 mL, 469 mmol) were dissolved in diethyl ether (230 mL) in air. The solution was cooled to 0°C and stirred for 16 h, after which the solvent was removed via rotary evaporation to give a yellow/white solid. The

product was treated with 2 M NaOH (200 mL) and extracted with hexane (4 x 100mL). The mixture was dried over anhydrous MgSO₄, gravity filtered, and the solvent was removed via rotary evaporation to give an orange oil. The product was flash distilled at 90 °C under vacuum to give **1** as a yellow oil. Yield: 9.94 g, 34.8 mmol, 62%. ¹H-NMR (CDCl₃, ppm): 7.39–7.13 (3H, m, CH), 3.54 (4H, s, CH₂N), 2.30 (12H, s, NMe₂) (**Figure A.1**).

2.3 Synthesis of (NCN)InMe₂ (**2**)²⁵

N-BuLi (3.50 mL, 11.1 mmol) was added to a solution of (NCN)Br (3.00 g, 11.1 mmol) in hexane (32 mL) to give a yellow/orange cloudy solution. The reaction mixture was allowed to stir for 1 h, after which it was added dropwise to a suspension of Me₂InCl (2.00 g, 11.0 mmol) in hexane (20 mL). After stirring for 16 h, the solution was cloudy white. The reaction mixture was filtered, and the solvent was removed under reduced pressure to afford **2** as a beige powder. Yield: 0.42 g, 10.0 mmol, 91%. ¹H NMR (ppm, CDCl₃): 7.01 (1H, t, *J* = 2 Hz, CH), 6.85 (2H, d, *J* = 7 Hz, CH), 3.41 (4H, s, CH₂N), 2.19 (12H, s, NMe₂), -0.54 (6H, s, InMe₂) (**Figure A.2**).

2.4 Synthesis of H₂(NO) (**3**)^{26,27}

Tert-butylamine (1.65 g, 22.5 mmol) was added to a solution of 3-6-di-*tert*-butylcatechol (5.00 g, 22.5 mmol) in acetonitrile (150 mL). Following the addition of 3Å molecular sieves (10 g), the solution was heated at reflux for 16 h with a drying column. The reaction mixture was suction filtered, and the product was washed with diethyl ether. The resulting filtrate was then dried under reduced pressure to afford a green solid. The product was redissolved in diethyl ether (100 mL) and added to a separatory funnel along with a solution of sodium hydrosulfite (3 g) in distilled water (200 mL). With each wash (x3), the solution turned clear brown. The organic layer was collected and dried over anhydrous magnesium sulfate. The solution was gravity filtered and

the solvent removed under reduced pressure. The product was redissolved in dry acetonitrile (50 mL) and the solution cooled to -15°C . After 16 h, the crystalline product **3** was collected by filtration. Yield: 1.86 g, 6.70 mmol, 30%. ^1H NMR (ppm, CDCl_3): 7.13 (1H, d, $J = 2$ Hz, *NH*), 6.95 (1H, d, $J = 2$ Hz, *CH*), 1.41 (9H, s, *CtBu*), 1.27 (9H, s, *NtBu*), 1.17 (9H, s, *CtBu*) (**Figure A.3**).

2.5 Synthesis of $(\text{NC})\text{InMe}_2$ (**4**)

N-BuLi (3.75 mL, 6.00 mmol) was added to a colourless solution of dimethylbenzylamine (0.676 g, 5.00 mmol) in diethyl ether (20 mL) causing the solution to immediately turn bright pink. After stirring for 15 min, the solution turned golden yellow. After stirring for a total of 16 hr, the solution became cloudy. The reaction mixture was then added dropwise to a solution of InMe_2Cl (0.902 g, 5.00 mmol) in diethyl ether (10 mL) to give a cloudy white solution. The solution was stirred for 3 h, after which the solvent was removed under reduced pressure to give a yellow/white gel. The gel was redissolved in pentane (6 mL) to give a cloudy white solution. The solution was filtered, and the solvent was removed under reduced pressure yielding **4** as a yellow/brown oil. Yield: 1.06 g, 25.0 mmol, 80%. ^1H NMR (ppm, CDCl_3): 7.14-7.26 (3H, m, *CH*), 3.71 (2H, s, CH_2N), 2.47 (6H, s, NMe_2), 0.22 (6H, s, *InMe*) (**Figure A.4**).

2.6 Synthesis of $(\text{NCN})\text{InCl}_2$ (**5**)²⁸

N-BuLi (7.00 mL, 11.06 mmol) was added to a clear yellow solution of **1** (3.00 g, 11.0 mmol) in THF (32 mL) to give an orange solution. After stirring for 1 h, the reaction mixture was decanted into a solution of InCl_3 (2.45 g, 11.06 mmol) in THF (32 mL) resulting in a clear yellow solution. The reaction mixture was stirred for 16 h, then the solvent was removed under reduced pressure to give a thick yellow oil. The product was dissolved in toluene (5 mL), the mixture was

filtered, and the solvent was removed under reduced pressure to give a brown solid. The product was washed with hexane (10 mL) and the hexane removed to give **5** as a fine white powder. Yield: 2.63 g, 6.96 mmol, 63%. $^1\text{H NMR}$ (ppm, CDCl_3): 7.27 (1H, q, $J = 7$ Hz, CH), 7.04 (2H, d, $J = 7$ Hz, CH), 3.60 (4H, s, CH_2N), 2.51 (12H, s, NMe_2) (**Figure A.5**).

2.7 Synthesis of (Me)In(NO) (**6**)²⁹

A solution of **3** (0.264 g, 0.952 mmol) in diethyl ether (3 mL) was added dropwise to a solution of InMe_3 (0.152 g, 0.952 mmol) in diethyl ether (4 mL). The reaction mixture bubbled upon addition, giving a light brown clear solution. After stirring for 3 h, the reaction mixture was filtered to give a clear yellow solution. The solution was allowed to sit at 23°C for 16 h and after which colorless crystals and powder of **6** was collected by filtration in low yield. $^1\text{H NMR}$ (ppm, CDCl_3): 7.12 (1H, d, CH), 6.88 (1H, d, CH), 6.48 (1H, s, CH), 1.28 (27H, m, *CtBu* & *NtBu*), 0.45 (3H, s, *InMe*) (**Figure A. 16**).

2.8 Synthesis of (NCN)In(HNO)₂ (**7**)

A solution of **3** (0.382 g, 1.38 mmol) in diethyl ether (18 mL) was cooled to -78°C . *N*-BuLi (1.7 mL, 2.75 mmol) was added dropwise, giving a bright yellow solution of $\text{Li}_2(\text{NO})$. The reaction mixture was allowed to stir for 30 min then added dropwise at 23°C to a solution of **5** (0.519 g, 1.38 mmol) in diethyl ether (10 mL), giving a cloudy yellow solution. After stirring for 16 h, the reaction mixture was filtered to remove a yellow powder. The solvent was removed under reduced pressure to give a brown solid. The product was redissolved in pentane (5 mL) and filtered to remove **7** as a white powder. The filtrate was stored at -15°C for 16 h, after which **7** was collected by filtration as colorless crystals and green powder. Yield: 0.28 g, 0.33 mmol, 35%. Elemental Analysis: Calculated: C: 67.12%, H: 9.27%, N: 6.52%. Found: C: 67.50%, H: 8.82%, N: 6.80%.

^1H NMR (ppm, CDCl_3): 7.18 (3H, m, aryl H NCN), 6.35 (4H, d, aryl H NO), 3.54 (4H, m, CH_2N), 2.31 (4H, d, NMe_2), 1.30 (54H, m, $t\text{Bu}$) (**Figure A.7**). $^{13}\text{C}\{^1\text{H}\}$ (ppm, CDCl_3): 158.66, 151.24, 149.17, 144.62, 143.47, 136.67, 133.86, 129.84, 128.15, 126.64, 125.53, 122.90, 121.57, 112.37, 110.02, 77.14, 66.06, 64.35, 57.65, 45.49, 33.93, 31.65, 29.49, 22.37, 14.14 (**Figure A.8**). FT-IR (cm^{-1}): 2952 (s), 2866 (s), 2788 (w), 1444.34 (broad), 1416 (s), 1383 (w), 1360 (m), 1301 (w), 1254 (broad), 1254 (w), 1231 (m), 1200 (m), 1173 (w), 1126 (w), 1019 (w), 970 (m), 877 (w), 846 (m), 827 (m), 739 (m), 652 (w) (**Figure A.9**). Melting point: 121-125°C.

2.9 Synthesis of $(\text{NCN})\text{In}(\text{NO})$ (**8**)

A solution of **3** (0.382 g, 1.38 mmol) in diethyl ether (18 mL) was cooled to -78°C . $N\text{-BuLi}$ (1.7 mL, 2.75 mmol) was added dropwise giving a bright yellow solution of $\text{Li}_2(\text{NO})$. The reaction mixture was immediately added dropwise to a 23°C solution of **5** (0.519 g, 1.38 mmol) in diethyl ether (10 mL), giving a cloudy yellow solution. After stirring for 3 h, the reaction mixture was filtered to remove a yellow powder. The solvent was removed under reduced pressure to give a brown solid. The product was redissolved in pentane (5 mL) and filtered to remove **8** as a white/beige powder. The filtrate was concentrated to 2 mL and allowed to sit at 23°C . After 16 h, colorless crystals of **8** were collected by filtration. Yield: 0.42 g, 0.72 mmol, 52%. Elemental Analysis: Calculated: C: 61.96%, H: 8.32%, N: 7.23%. Found: C: 61.69% H: 8.08% N: 7.47%. ^1H NMR (ppm, CDCl_3): 7.04 (2H, m, aryl H), 6.63 (1H, m, CH), 3.58 (4H, q, CH_2N), 2.26 (4H, m, NMe_2), 1.35 (9H, m, $t\text{Bu}$) (**Figure A.10**). $^{13}\text{C}\{^1\text{H}\}$ (ppm, CDCl_3): 158.65, 151.98, 144.60, 143.98, 142.94, 134.36, 131.08, 129.28, 128.04, 125.83, 121.57, 108.80, 106.94, 77.13, 66.12, 63.71, 51.72, 45.47, 35.07, 34.30, 33.69, 32.21, 30.17, 29.71, 28.84 (**Figure A.11**). FT-IR (cm^{-1}): 2981 (broad), 2958 (w), 2872 (broad), 2836 (w), 2793 (w), 1581 (w), 1450 (m), 1354 (w), 1248 (w),

1205 (w), 1102 (w), 1002 (s), 952 (w), 844 (s), 777 (s), 710 (w), 617 (w) (**Figure A.12**). Melting point: 216°C.

2.10 Synthesis of (NCN)InI₂ (**9**)

A cloudy yellow solution of **8** (0.250 g, 0.430 mmol) in diethyl ether (3 mL) was added dropwise to a solution of diiodine (0.109 g, 0.430 mmol) in diethyl ether (3 mL) resulting in a clear green solution. After a 30-minute stir, the solution was allowed to sit at 23°C for 16 h. Colorless crystals of **9** were collected by filtration. Yield: 0.119 g, 0.213 mmol, 57%. ¹H NMR (ppm, CDCl₃): 7.22 (3H, aryl *H*), 3.53 (4H, m, CH₂N), 2.49 (12H, s, NMe₂) (**Figure A.17**). ¹³C{¹H} NMR (ppm, CDCl₃): 142.71, 129.57, 125.65, 76.41 63.12, 46.60 (**Figure A.18**). FT-IR (cm⁻¹): 2952 (broad), 2869 (broad), 2793 (w), 1649 (w), 1624 (w), 1449 (m), 1378 (w), 1271 (w), 1207 (m), 1001 (m), 902 (w), 842 (m), 773 (m), 618 (w) (**Figure A.19**). Melting point: 113°C.

2.11 Attempted synthesis of (NCN)In(NO)₂ (**12**)

8 (0.301 g, 0.516 mmol) was dissolved in diethyl ether (10 mL) to give a cloudy yellow solution. Dry O₂ was then bubbled through the stirred solution for 10 min to produce a dark green solution. The solvent was removed under reduced pressure and the product was redissolved in pentane. The solution was allowed to sit at 23°C under a dinitrogen atmosphere for 16 h, after which tiny needle-like colorless crystals of **12** were collected by filtration. Yield: 0.155 g, 0.181 mmol, 52%. Melting point: 221°C.

2.12 Cyclic Voltammetry

Cyclic voltammetry experiments were conducted to test the electrochemistry of (NCN)In(NO). This was performed in a glove box using a PC-interfaced BASi Epsilon Eclipse potentiostat and proprietary software (version 3.0.84). Both a platinum wire counter electrode and

a platinum-disk working electrode were used in a 10 mL three-neck round bottom flask in order to conduct this experiment. The potentials applied throughout were referencing a reversible ferrocene wave (Fc/Fc^1). Here, the observed half-wave potential for this couple $E_{1/2} = + 0.081 \text{ V}$ was subtracted, this then could be converted to potential vs SCE by adding 0.380 V to the resulting value. Analyte concentrations used throughout were 1 mM, while the supporting electrolyte used was 0.1 M $[\text{NBu}_4][\text{PF}_6]$. All cyclic voltammetry experiments were conducted in acetonitrile under a dinitrogen atmosphere at 23°C.

2.13 Computational methods (NCN)In(NO) (**8**)³¹

Density functional theory (DFT) calculations were performed using Gaussian 16 Revision C.01 at the PBE1PBE-GD3BJ/def2-TZVP level of theory for all atoms except for indium and iodine, for which Stuttgart electron core pseudo-potentials (SDD) were employed. Solid-state structures of **8** and **9** obtained by X-ray crystallography were used as starting points in geometry optimizations when possible. All other structures were geometry-optimized and structural parameters for input files were adapted from crystal structure data. Frequency calculations were performed on all structures to verify minima with no imaginary frequencies were obtained. Dispersion corrections were included throughout using the D3 empirical correction from Grimme with Becke-Johnson dampening (GD3BJ). All energies reported herein are the sum of the total gas-phase electronic energies plus enthalpic thermal corrections at 298 K.

2.14 X-ray Crystallography

Crystals of compounds **7-9** were mounted from Paratone-N oil on a MiTeGen MicroMount. The data was collected on a Bruker APEX II charge-coupled-device (CCD) diffractometer, with an Oxford 700 Cryocool sample cooling device. The instrument was equipped with graphite-

monochromated Mo K α radiation ($\lambda=0.71073\text{\AA}$; 30 mA, 50 mV), with Monocap X-ray source optics. Upon data collection, our ω -scan frame series were collected with 0.5° wide scans, 5 second frames and 366 frames per series at varying φ angles ($\varphi=0^\circ, 90^\circ, 180^\circ, 270^\circ$). Data collection, unit cell refinement, data processing and multi-scan absorption correct were applied using the APEX2, APEX3 or APEX4 software packages. The structures were solved using SHELXT and all non-hydrogen atoms were refined anisotropically with SHELXL using a combination of shelXle and OLEX2 graphical user interfaces. Unless otherwise noted, all hydrogen atom positions were idealized and ride on the atom to which they were attached. The final refinement included anisotropic temperature factors on all non-hydrogen atoms. Details of crystal data, data collection and structure refinement are listed in **Tables 1**. All figures were generated using Diamond software.

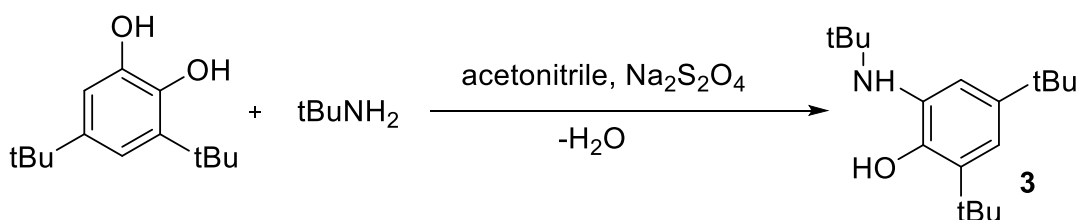
Table 1: Crystallographic data for Compounds **7-9**.

Molecular Formula	$C_{48}H_{79}InN_4O_2$	$C_{30}H_{48}InN_3O$	$C_{12}H_{19}I_2InN_2$
Formula Weight (g/mol)	858.97	581.53	559.92
Crystal System	Monoclinic	Monoclinic	Monoclinic
Space Group	C2/c	P2 ₁ /c	P -1
<i>a</i> (Å)	20.1892(7)	10.2953(4)	8.8911(4)
<i>b</i> (Å)	23.6428(8)	11.6773(4)	11.3916(4)
<i>c</i> (Å)	10.2543(3)	25.7983(9)	16.8104(6)
α (deg)	90	90	87.119(1)
β (deg)	102.1120(10)	97.9540(10)	88.413(1)
γ (deg)	90	90	84.537(1)
<i>V</i> (Å ³)	4785.7(3)	3071.67(19)	1692.30(11)
<i>Z</i>	4	4	4
F (000)	1840.0	1224.0	1040.0
ρ (g/cm ³)	1.192	1.258	2.198
μ (mm ⁻¹)	0.533	0.794	5.030
<i>T</i> (K)	150	150	150

3. Results and Discussion

3.1 Synthesis of H₂(NO) (**3**)

The procedure outlined by Ringenburg et al.²⁶ and modified from Blackmore et al.²⁷ was followed for the synthesis of H₂(NO). This entailed reacting *tert*-butylamine with 3,6-di-*tert*-butylcatechol in acetonitrile to give a light brown solution (**Scheme 2**). After the addition of molecular sieves, the reaction mixture was then set to reflux at 80 °C for 16 h. During this time, the reaction mixture changed from light brown to a dark green solution. The reaction mixture was then suction filtered, and the sieves were washed with diethyl ether. The combined solutions were then dried under reduced pressure to afford a dark green solid. After redissolving in diethyl ether (100 mL), the organic layer was added to a separatory funnel and washed with a solution of sodium hydrosulfite and distilled water. After each wash the reaction mixture (organic layer) changed from green to brown, indicating reduction of the amidophenolate. The organic layer was then collected and dried and the solvent was removed under reduced pressure. The product was then recrystallized from acetonitrile, yielding a green solid.



Scheme 2: Reaction scheme for the synthesis of H₂(NO) (**3**).

It was determined through ¹H NMR spectroscopy that this dark green solid was not H₂(NO) (**3**), as the chemical shifts and integration did not agree with literature values.^{26,27} It was concluded that the colour change from brown to green that occurred during crystallization at -15 °C (freezer)

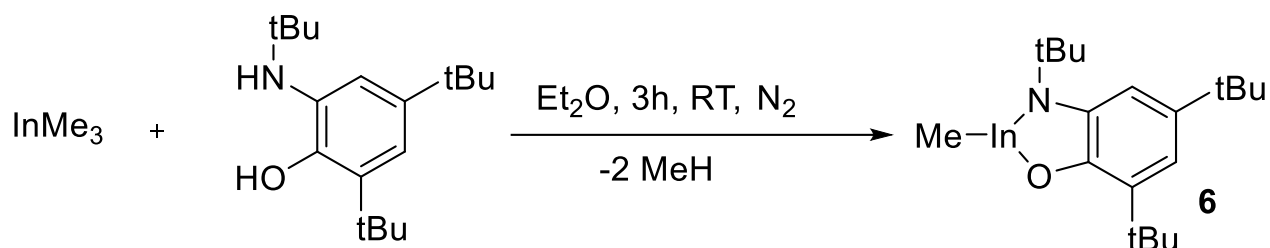
were indicative of hydrolysis, indicating that **3** is both very air and moisture sensitive. Recrystallization of the product at 23°C in the glove box circumvented this issue and **3** was successfully isolated as a brown powder pebble-like solid in a 30% yield. The ¹H NMR spectrum (**Figure A.3**) was consistent with literature values.

3.2 Synthesis of (Me)In(NO) (**6**)

Various procedures were attempted to synthesize (Me)In(NO) (**6**). Initial attempts consisted of a hydrocarbon elimination reaction where H₂(NO) (**3**) was added dropwise to a reaction mixture of Me₃In in toluene. This addition caused bubbling and a color change from colourless to a brown/yellow-like solution. The reaction mixture was set to reflux at 110°C for 3 h, yielding a green solution. Attempted crystallization of the product from the reaction solvent, at -15 °C afforded a microcrystalline product and a brown goop-like reaction mixture. The crystalline material was found not to be of X-ray crystallography quality. Further, the green color change that occurred throughout the reflux could be indicative of hydrolysis, similar to what had been previously observed during the recrystallization of **3**, once again emphasizing the air and moisture sensitivity of these compounds. It was also postulated that heating the reaction at reflux (110°C) may be causing the product to decompose.

Future attempts of this reaction was performed in diethyl ether and closely followed the procedure developed by Piskunov et al.³⁰ This time, the H₂(NO) (**3**) was added to a solution of trimethylindium in diethyl ether (**Scheme 3**). The reaction mixture again bubbled and resulted in a clear yellow solution. The reaction mixture was stirred for 3 h during which there were no observed colour changes. The reaction mixture was concentrated and allowed to sit at room temperature. After 16 h, crystalline material had formed at the bottom of the reaction mixture. To confirm the identity of the product, a ¹H NMR spectrum of the crystalline material was collected

(Figure A.16). The ^1H NMR spectrum agreed with theoretical values for $(\text{Me})\text{In}(\text{NO})$ (**6**), with the peak of utmost interest being the indium-methyl singlet peak found at 0.45 ppm and integrating for 3H. The reaction was then repeated at a larger scale where **6** was isolated as both powder and crystalline material in low yield. However, the crystalline material was not suitable for X-ray crystallography.

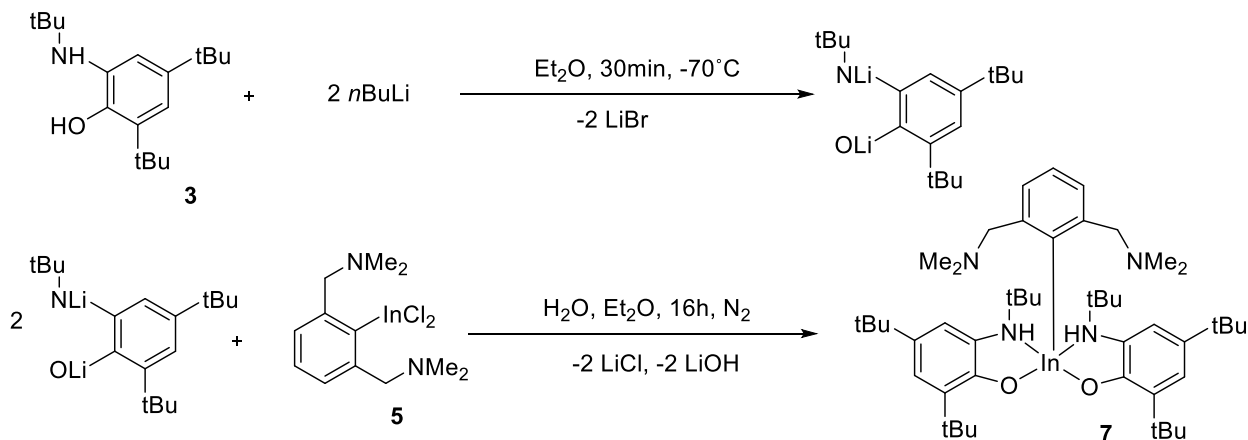


Scheme 3: Reaction scheme for the synthesis of $(\text{Me})\text{In}(\text{NO})$ (**6**).

3.3 Synthesis of $(\text{NCN})\text{In}(\text{HNO})_2$ (**7**)

The synthesis of $(\text{NCN})\text{In}(\text{NO})$ first involved lithiating the amidophenolate ligand (**3**) with *n*-BuLi and allowing for a 30-minute stir in a cold bath (-78°C) (Scheme 4). The resulting yellow solution was then added dropwise to a solution of $(\text{NCN})\text{InCl}_2$ (**5**) in diethyl ether and stirred for 16 h. Colourless crystals and a green powder precipitated out of the green pentane reaction mixture after sitting at room temperature for 16 h. The ^1H NMR spectrum of the product indicated larger than expected integration values for the NO ligand peaks. The crystalline material was subsequently sent for X-ray crystallography where it was determined to be $(\text{NCN})\text{In}(\text{HNO})_2$ (**7**). This was indicative that hydrolysis was once again occurring as the amido groups were protonated during the reaction. Compound **7** was characterized using ^1H NMR (Figure A.7), $^{13}\text{C}\{^1\text{H}\}$ NMR (Figure A.8), FT-IR (Figure A.9) and X-ray crystallography (Figure 7). However, reactivity was not assessed due the inactive redox properties of this compound. The synthesis of **7** was repeated

using the appropriate stoichiometry of two equivalents of **3**, two equivalents of *n*-BuLi and one equivalent of **5**. The adapted procedure yielded colorless crystals from the clear green diethyl reaction mixture in a 35% yield.



Scheme 4: Reaction scheme for the synthesis of (NCN)In(HNO)₂ (**7**).

3.4 X-ray crystal structure of (NCN)In(HNO)₂ (**7**)

The crystalline product of (NCN)In(HNO)₂ (**7**) was analysed by X-ray crystallography and the structure is shown in **Figure 7**. The two H(NO) ligands are chelating the indium centre while nitrogen atoms (N1 and N1*) of the NCN pincer ligand are not bonded to the indium metal centre. The indium is in a distorted square pyramidal bonding environment with a NCN carbon atom (C1) in the apical position and the H(NO) oxygen atoms (O1 and O1*) and nitrogen atoms (N1 and N1*) in basal position.

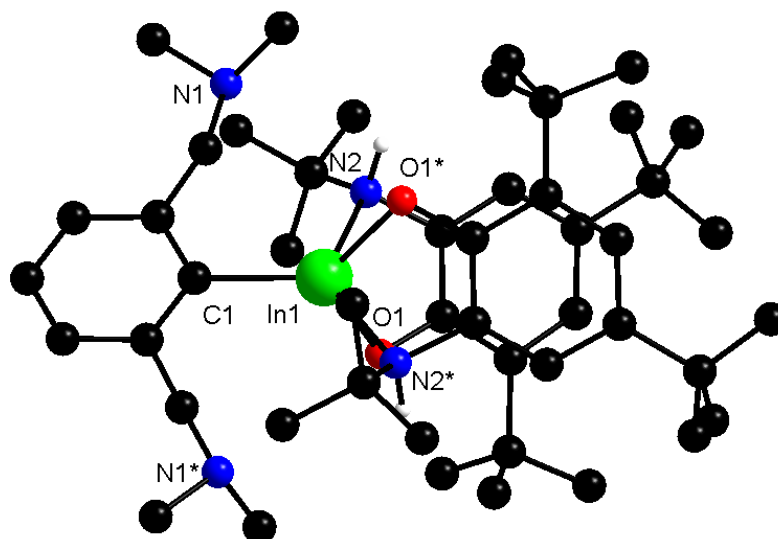


Figure 7: X-ray crystal structure of (NCN)In(HNO)₂. Hydrogen atoms are removed for clarity.

Selected bond distance (Å) and angles (°): In(1)-O(1) = 2.109(2), In(1)-O(1)* = 2.109(2), In(1)-N(2) = 2.377(2), In(1)-N(2)* = 2.377(2), C(1)-In(1) = 2.162(4), O(1)*-In(1)-O(1) = 115.94(11), O(1)*-In(1)-N(2) = 81.37(9), O(1)*-In(1)-N(2)* = 74.21(8), O(1)-In(1)-N(2)* = 81.36(9), O(1)-In(1)-N(2) = 74.21(8), O(1)*-In(1)-C(1) = 122.03(6), O(1)-In(1)-C(1) = 122.03(6), N(2)-In(1)-N(2)* = 133.09(12), C(1)-In(1)-N(2) = 113.46(6), C(1)-In(1)-N(2)* = 113.46(6).

3.5 Synthesis of (NCN)In(NO) (**8**)

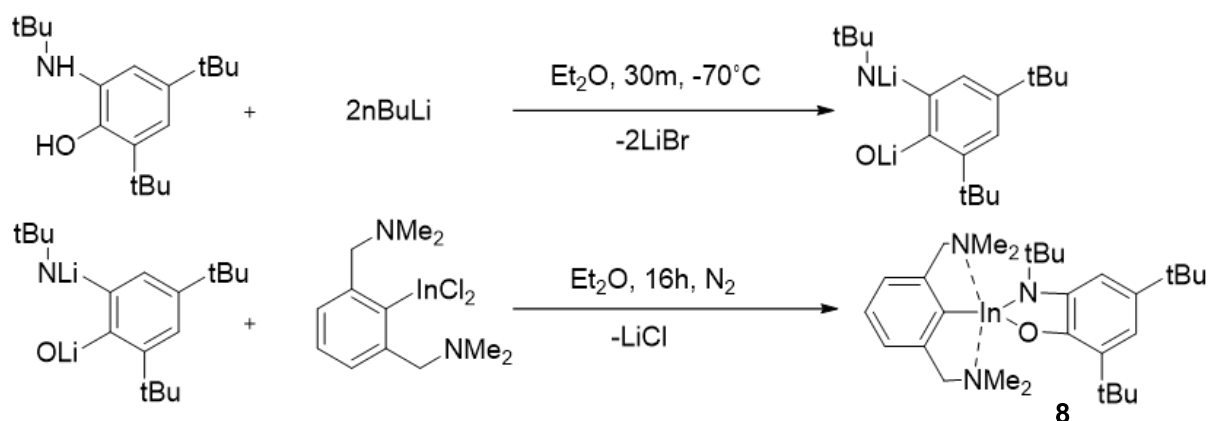
There were various attempts made to synthesize (NCN)In(NO) (**8**). Following the unexpected synthesis of (NCN)In(HNO)₂ (**7**), an optimized procedure to synthesize (NCN)In(NO) was developed (**Scheme 5**). After addition of **3** and **5**, the reaction was heated at reflux for 16 h. A common challenge that arose was that the resulting solution turned dark green. This colour change was indicative of oxidation despite carrying out the reaction under dinitrogen atmosphere on a Schlenk line. Once the green reaction mixture was concentrated, the solution turned to a goop-like consistency causing isolation issues. The procedure was then altered to include a controlled

heating involving an increase in temperature every 30 minutes to reflux to observe when the colour change was occurring. However, even after these alterations the reaction mixture turned green and yielded only microcrystalline material.

Due to the unsuccessful previous procedure, it was decided all steps would be performed under a dinitrogen atmosphere. To start, **3** was added to sodium hydride in THF. This was allowed to stir for 30 minutes, producing $\text{Na}_2(\text{NO})$ and H_2 . This resulting solution was added to a solution containing **5** in THF and the reaction mixture was allowed to stir for 16 h. The solution was filtered to remove NaCl and resulted in a clear colorless solution. The solvent was then removed under reduced pressure to yield a green oil and again causing product isolation issues. The reaction mixture was washed with hexane and the solvent was removed once again. Unfortunately, the reaction mixture resulted in a green oil once again. The product was allowed to crystallize from hexane, affording a microcrystalline product. The ^1H NMR spectrum included unidentifiable peaks indicating that the target product **8** had not been synthesized. X-ray crystallography revealed that the product was contaminated with the reactant $(\text{NCN})\text{InCl}_2$ (**5**).

Various solvents such as toluene, tetrahydrofuran, hexane, pentane and diethyl ether were used in attempts to find that best suited for solubility and crystallization of the target product. A final procedure (**Scheme 5**) consisted of lithiating $\text{H}_2(\text{NO})$ in diethyl ether with *n*-BuLi in a cold bath (-78°C). The golden yellow solution was then added dropwise to a solution containing **5** in diethyl ether to result in a yellow/orange cloudy solution. The reaction mixture was allowed to stir for 3h. After unsuccessfully attempting to crystallize the product directly from the reaction mixture, the solvent was removed under reduced pressure and pentane (5 mL) was added. After the removal of LiCl , both a beige powder and colorless crystalline material precipitated from solution. The mixture was filtered and the filtrate was allowed to sit at room temperature for 16 h.

X-ray quality crystals formed from the pentane solution, which was then sent for X-ray crystallography and were confirmed the target product (NCN)In(NO) (**8**) (**Figure 8**). Both the powder-like material and the crystalline material were confirmed to be **8** by ^1H NMR (**Figure A.10**), $^{13}\text{C}\{^1\text{H}\}$ NMR (**Figure A.11**) FT-IR (**Figure A.12**) and X-ray crystallography (**Figure 7**). The optimized procedure yielded colorless crystals of **8** in a 52% yield.



Scheme 5: Reaction scheme for the synthesis of (NCN)In(NO) (**8**).

3.6 X-ray crystal structure of (NCN)In(NO) (**8**)

The X-ray crystal structure of (NCN)In(NO) (**8**) is presented in **Figure 8**. The nitrogen atoms (N1 and N2) and the carbon atom (C1) of the NCN pincer ligand are bonded to the indium metal centre, as well as the nitrogen (N3) and oxygen (O1) of the chelating NO ligand. The indium centre is in a distorted trigonal bipyramidal bonding environment with the amidophenolate N3 and O1 atoms and the NCN ligand and C1 atom in equatorial sites, and the NCN pincer ligand N1 and N2 atoms in axial positions.

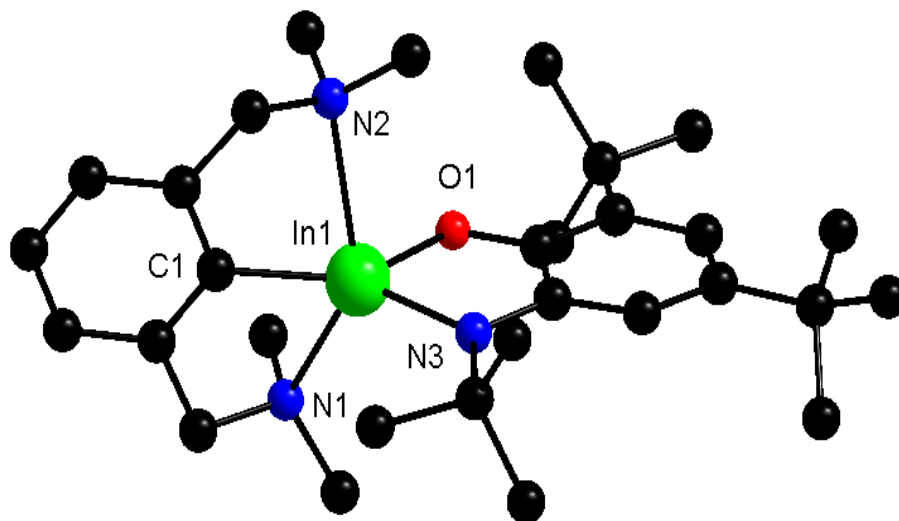
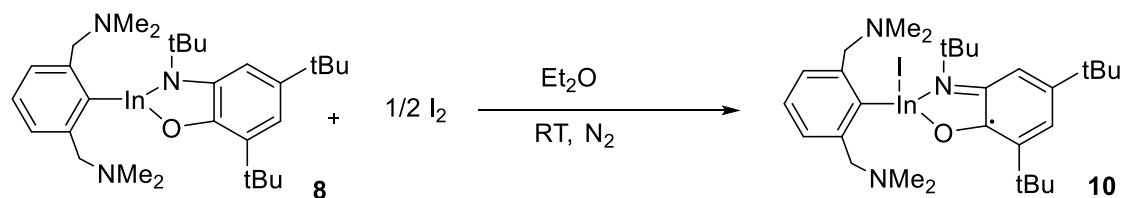


Figure 8: X-ray crystal structure of (NCN)In(NO). Hydrogen atoms removed for clarity. Selected bond distance (Å) and angles (°): In(1)-O(1) = 2.0541(7), In(1)-N(1) = 2.4836(9), In(1)-N(2) = 2.4976(9), In(1)-N(3) = 2.0679, In(1)-C(1) = 2.1108(10), O(1)-In(1)-N(1) = 91.98(3), O(1)-In(1)-N(2) = 92.61 (3), O(1)-In(1)-N(3) = 82.49(3), O(1)-In(1)-C(1) = 139.90(4), N(1)-In(1)-N(2) = 136.57 (3), N(3)-In(1)-N(1) = 117.18(3), N(3)-In(1)-N(2) = 106.23(4), N(3)-In(1)-C(1) = 137.34(4), C(1)-In(1)-N(1) = 74.81(4), C(1)-In(1)-N(2) = 74.16(4).

3.7 Reaction of (NCN)In(NO) (8) with Diiodine

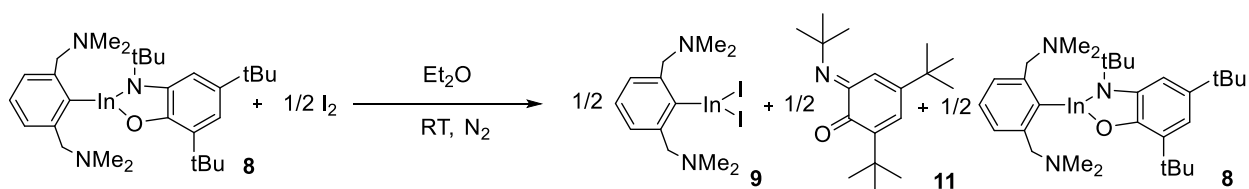
The reactivity of (NCN)In(NO) (**8**) was probed using diiodine (I₂) as a mild oxidizing agent. A cloudy yellow solution of (NCN)In(NO) in diethyl ether was added dropwise to a solution of diiodine in diethyl ether which resulted in a clear green solution. After a 30-minute stir, the solution was allowed to sit at 23°C for 16 h after which, colorless crystals and powder-like material of **9** were collected by filtration. The ¹H NMR spectrum of (**9**) showed that there were no longer any peaks reflecting the coordinated amidophenolate ligand (**3**) (**Figure A.14**). The expected synthetic product is shown in **Scheme 6**, where a one-half equivalent of diiodine is reacted with (**8**), to form the [(NCN)InI(NO)][•] radical (**10**).



Scheme 6: The expected synthetic route of the oxidation of (NCN)In(NO) with iodine.

This reaction was further studied using a small scale ¹H NMR experiment in CDCl₃. Upon addition of one-half an equivalent of diiodine, the colour of the reaction mixture changed from yellow to light green, indicative that **8** had been oxidized. This addition was repeated until there were a total of 1.5 equivalents of diiodine added to the reaction mixture. The solution became dark green after addition of 1 equivalent of diiodine and brown after addition of 1.5 equivalents. Once the solution turned brown, it was concluded that **8** was no longer reacting as the solution reflected the brown colour of elemental iodine.

After completion of the small scale ¹H NMR experiment, a preparative scale reaction of **8** with 0.5 equivalents of I₂ was performed (**Scheme 7**). The diethyl ether solvent was removed under reduced pressure which resulted in a green oil that was redissolved in pentane. After letting the solution sit for 16 h at room temperature, the green solution precipitated colourless crystals. The crystalline material was sent for X-ray crystallography and was determined to be (NCN)InI₂ (**9**).



Scheme 7: Chemical oxidation of **8** with 1/2 equivalents of I₂ resulting in the formation of (NCN)InI₂ (**9**).

The amidophenolate ligand is capable of undergoing a two-electron oxidation (**Figure 3**).¹⁸ The synthesis of (NCN)InI₂ (**9**) from the reaction of **8** with 0.5 equivalents of I₂ suggests that the dianionic amidophenolate ligand undergone a two-electron oxidation in half of the reactant, resulting in the neutral iminobenzosemiquinone (**11**) and unreacted **8** (**Scheme 7**). This differs from the expected one-electron oxidation of the amidophenolate ligand to produce the iodoindium amidophenolate product [(NCN)InI(NO)]⁺ (**10**), as reported for similar RIn(ON) compounds in the literature (**Scheme 6**).³⁰ The reaction was repeated using one equivalent of I₂ to allow complete reaction of **8** (**Scheme 8**). The pure product **9** was then characterized using ¹H NMR (**Figure A.17**), ¹³C{¹H} NMR (**Figure A.18**), FT-IR (**Figure A.19**) and X-ray crystallography (**Figure 9**).

3.8 X-ray crystal structure of (NCN)InI₂ (**9**)

The X-ray crystal structure of **9** is shown in **Figure 9**. The nitrogen atoms (N1 and N2) and the carbon atom (C1) of the chelating NCN pincer ligand are bonded to the indium metal centre, as well as two iodine atoms (I1 and I2). The indium centre is found to be in a distorted trigonal bipyramidal bonding environment with the iodine atoms I1 and I2 and the NCN ligand C1 atom in equatorial sites and the NCN pincer ligand N1 and N2 atoms in axial positions.

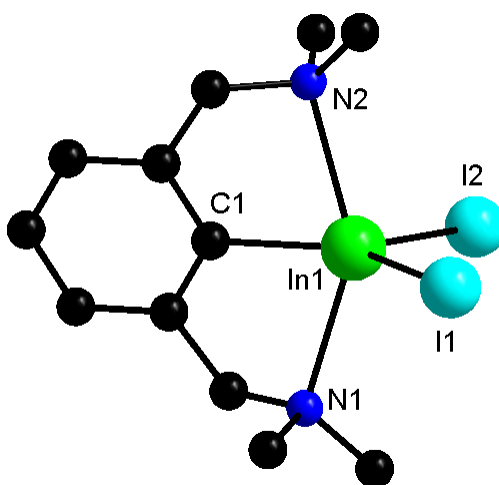


Figure 9: X-ray crystal structure of (NCN)InI₂ (**9**). Hydrogen atoms removed for clarity. Selected bond distance (Å) and angles (°): I(1)-In(1) = 2.7142(2), I(2)-In(1) = 2.6959(3), In(1)-N(1) = 2.496(2), In(1)-N(2) = 2.544(2), In(1)-C(1) = 2.114(2), I(2)-In(1)-I(1) = 107.045(9), N(1)-In(1)-I(1) = 97.68(5), N(1)-In(1)-I(2) = 97.50(5), N(1)-In(1)-N(2) = 148.42(7), N(2)-In(1)-I(1) = 101.18(5), N(2)-In(1)-I(2) = 100.84(5), C(1)-In(1)-I(1) = 131.42(6), C(1)-In(1)-I(2) = 121.44(6), C(1)-In(1)-N(1) = 74.43(8), C(1)-In(1)-N(2) = 74.09(8).

3.9 Computational Studies of (NCN)In(NO) (**8**)

Density functional theory (DFT) calculations were performed in order to rationalize why the products (NCN)InI₂ (**9**) and doubly oxidized iminobenzosemiquinone (**11**) were preferentially formed over the singly oxidized iodoindium amidophenolate product [(NCN)InI(NO)][•] (**10**).³⁰ (Schemes 8 and 6, respectively). The geometry optimized structures of **8**, **9**, **10** and **11** are shown in Figure 10.

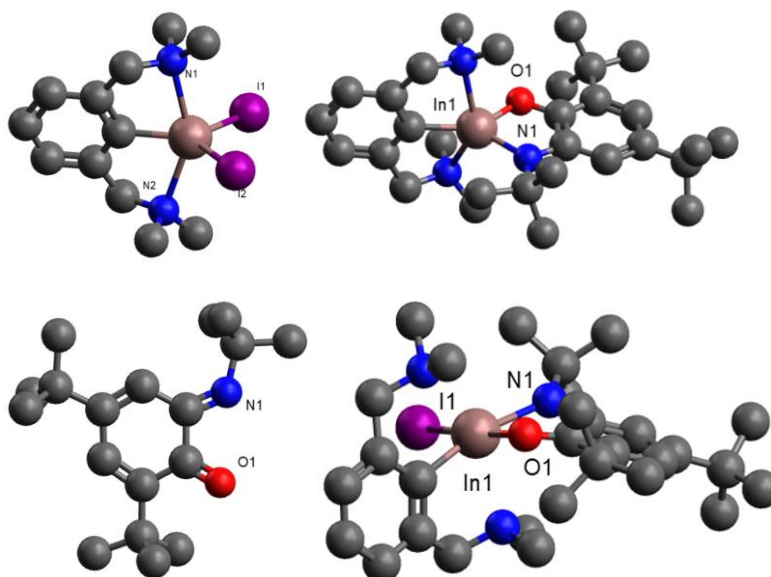
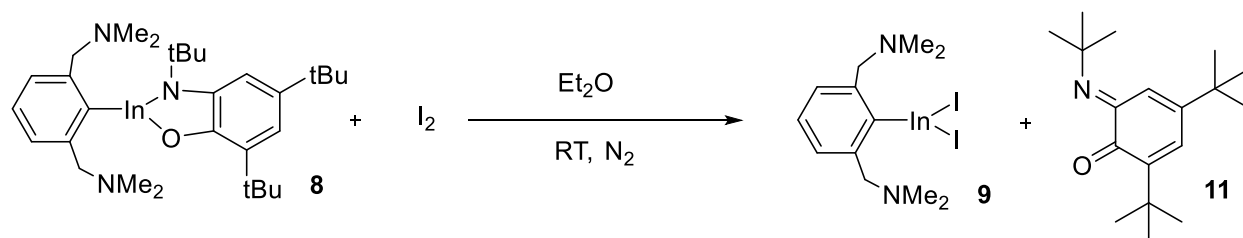


Figure 10: Geometry optimized structures of (NCN)In(NO) (**8**), (NCN)InI₂ (**9**), neutral iminobenzosemiquinone (**11**) and [(NCN)InI(NO)][•] (**10**). Hydrogen atoms are omitted for clarity.



Scheme 8: Chemical oxidation of **8** with 1 equivalent of I₂ resulting in the formation of (NCN)InI₂ (**9**).

Using the calculated total energy of each species, the energy of the reaction to form **9** and **11** was calculated to be -87.39 kJ/mol (**Scheme 8**). This value was compared to that of the reaction to form [(NCN)InI(NO)]^{*}, which was calculated to be -86.41 kJ/mol (**Scheme 6**). This suggests that the synthesis of (NCN)InI₂ (**9**) is only slightly more exothermic than that of [(NCN)InI(NO)]^{*} (**10**). This suggests that a very small kinetic barrier between the formation of **9** from the intermediate product **10** or that there is a lower kinetic barrier to the formation of **9** that does not involve **10** as an intermediate. Further, computational studies will be required to determine the mechanism of formation of **9**.

Both the reactivity and stability of a compound is directly related to its frontier orbitals, those being the HOMO (highest occupied molecular orbital) and the LUMO (lowest unoccupied molecular orbital). The HOMO of **8** shows that it is primarily located on the redox active amidophenolate ligand as expected (**Figure 11**). This suggested that that the oxidation of **8** should involve the amidophenolate ligand (**3**). Meanwhile the LUMO of **8** is located on the NCN pincer ligand.

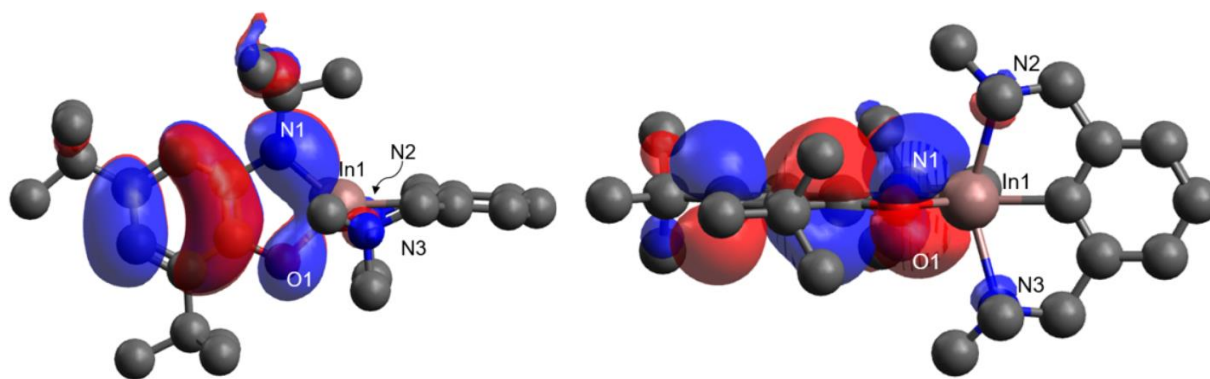


Figure 11: HOMO front view (left) and side view (right) of **8**.

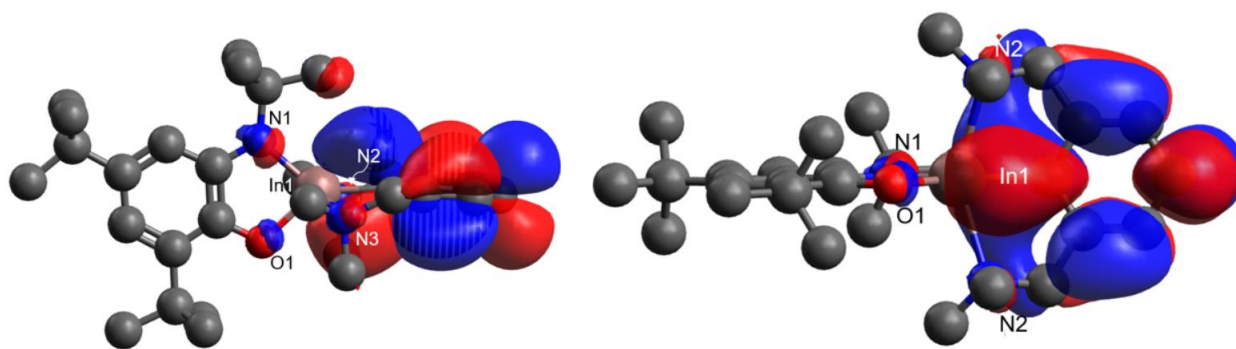
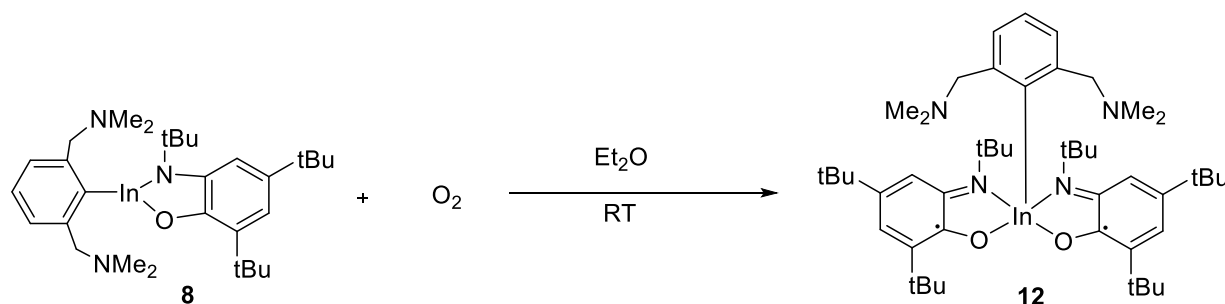


Figure 12: LUMO front view (left) and side view (right) of **8**.

3.10 Reaction of (NCN)In(NO) (**8**) with Dioxygen

The reactivity of (NCN)In(NO) (**8**) was further explored using dioxygen as an oxidizing agent. The proposed synthetic route is shown in **Scheme 9**. The expected formation of the product (NCN)In(NO)₂ (**12**) is based on the previously reported oxidation of APInI(TMEDA) with excess O₂ to give imSQ₂InI.³⁰ Excess dry oxygen was bubbled through a yellow solution of **8** in diethyl ether for 10 minutes, causing the reaction mixture to turn from yellow to dark green.. The solvent was removed under reduced pressure and the green solid was redissolved in diethyl ether and left to sit at room temperature to allow for crystallization. After 16 h under a dinitrogen atmosphere, the dark green solution had turned brown in colour and precipitated a powder-like material. The

colour change is indicative that the **8** has further reacted. The solvent was removed under reduced pressure, and the brown solid was redissolved in pentane in attempt to crystalline the material. The reaction mixture was once again allowed to sit for 16 h at room temperature, after which it precipitated needle-like crystals. The crystalline material was submitted for X-ray crystallography, but it was determined that the tiny needle-like crystals were not of suitable quality for analysis. Therefore, compound **8** shows evidence of reactivity with excess oxygen but the identity of the product remains unknown. The colorless powder-like material was characterized by ^1H NMR (**Figure A.20**), $^{13}\text{C}\{^1\text{H}\}$ NMR (**Figure A.21**) and FT-IR (**Figure A.22**).



Scheme 9: Chemical oxidation of **8** with O_2 resulting in the potential formation of $(\text{NCN})\text{In}(\text{NO})_2$ (**12**).

3.11 Cyclic Voltammetry of $(\text{NCN})\text{In}(\text{NO})$ (**8**)

Cyclic voltammetry (CV) was performed on the target compound, $(\text{NCN})\text{In}(\text{NO})$ (**8**) to assess its stability upon electrochemical oxidation. Throughout the CV experiment, a potential is applied through a solution containing **8** and a current flow is observed upon oxidation and/or reduction. Cyclic voltammetry experiments are performed using a three-electrode electrochemical cell. The three electrodes include the working electrode, reference electrode and the counter electrode. To test the chemical stability and reversibility, the applied potential at the working electrode was

varied in both forward and reverse directions at various scan rates, which then allowed for an observation of the current flow (**Figure 13**).

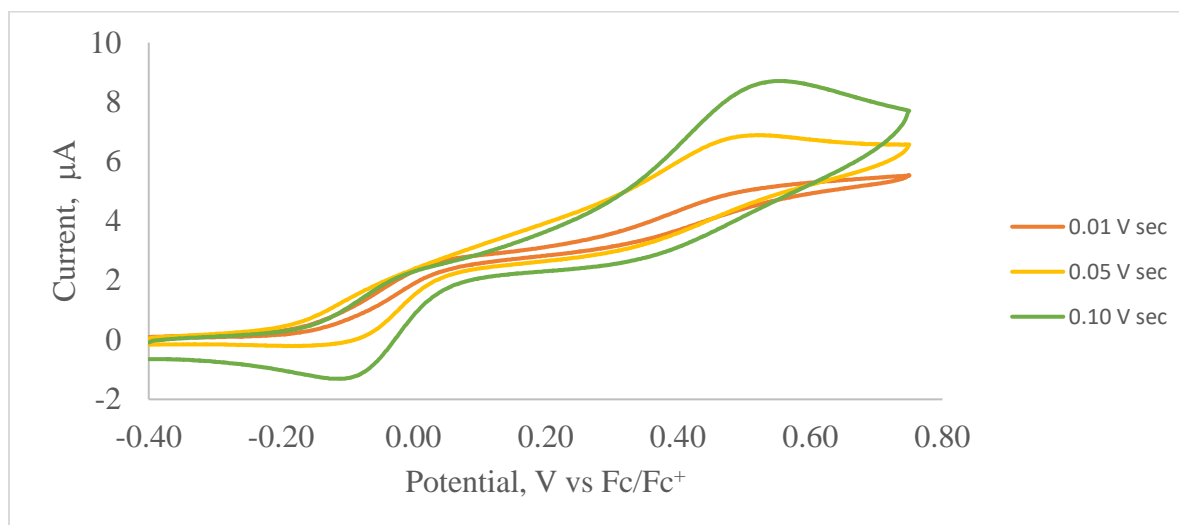


Figure 13: Cyclic voltammogram (0.01 V, 0.05 V, 0.10 V, 1 mM) of **8** in CH₃CN, 0.1 M [Bu₄][NPF₆], 23°C in acetonitrile under a dinitrogen atmosphere.

CV scans were collected at scan rates of 10, 50 and 100 mV/s (**Figure 13**). The resulting voltammograms show two oxidation peaks at ~0 mV and ~500 mV. The current of the peak at ~500 mV increases more rapidly than the peak at ~0 mV with increasing scan rate. This suggests that two different species in equilibrium are being oxidized, rather than a single compound being doubly oxidized. It is postulated that the two species are **8** and an acetonitrile solvated form **8**•MeCN (**Figure 14**). This oxidation appears to be followed by a chemical reaction and it does not appear to be reversible due to the lack of a corresponding reduction peak in the reverse direction.

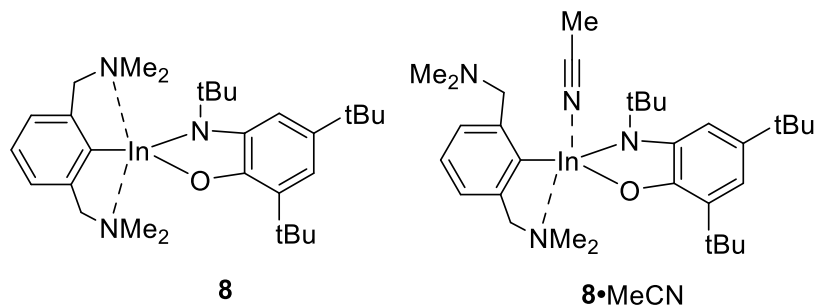
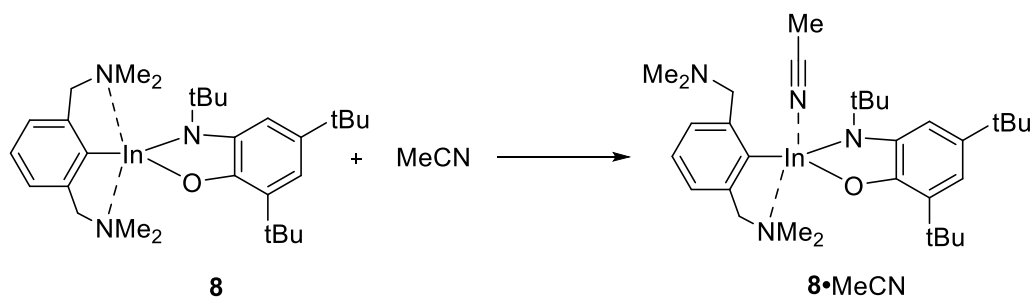


Figure 14: Chemical structures of (NCN)In(NO) (**8**) and its solvated form (NCN)In(NO)(MeCN) (**8•MeCN**).

Splitting of the CH_2N signal in the 1H NMR spectrum of **8** (Figure A.11) suggests a labile In-NMe₂ interaction with the NCN ligand where there is a second order multiplet found at 3.58 ppm. This signal suggests two inequivalent protons for the CH_2N fragment of the compound. The second order (AB) nature of this signal can be shown by the slanting of the peaks and large and inconsistent J values. When the NMe₂ is coordinated, the adjacent CH_2 cannot be exchanged via a symmetry element, being as the ligand is asymmetric, the protons are thus inequivalent and are found to be in different chemical environments. This presumably yields a solvated form where one of the respective NMe₂ groups on the pincer ligand is replaced by a coordinated CH₃CN molecule. To help justify this preliminary result, the energy of the reaction between **8** and MeCN to produce **8•MeCN** was found to be -2.81 kJ/mol (Scheme 10), suggesting that they are thermodynamically equivalent and in chemical equilibrium. The ionization energies of **8** and **8•MeCN** were calculated to be 354 kJ/mol and 388 kJ/mol, respectively, indicating that **8** has a lower ionization energy than the solvated form. The compound with the lower ionization energy will oxidize first as suspected. The resulting voltammogram therefore suggest that the first oxidation occurring at +0.5 V is reversible and reflective of the (NCN)In(NO) (**8**).



Scheme 10: Solvation of **8** with MeCN resulting in the formation of **8•MeCN**.

4. Conclusion

A procedure to reliably generate compounds **6-9** was successfully established. The X-ray crystal structure of **7** reveals a distorted square pyramidal bonding environment at the indium centre. The X-ray crystal structure of **8** reveals a distorted trigonal bipyramidal bonding environment similar to that of **9**. The preferential formation of **9** and doubly oxidized iminobenzosemiquinone **11** over the singly oxidized iodoindium amidophenolate product **10** from the reaction of **8** with diiodine was studied using computational studies, where it was found that formation of both products was exothermic with similar energies. The reactivity of **8** was further assessed using O₂ as an oxidizing agent. Preliminary evidence shows a reaction is occurring, but the products have not yet been characterized. The electrochemistry of **8** was studied using cyclic voltammetry where preliminary results suggest a chemical equilibrium between a solvated (**8**) and un solvated form (**8**•MeCN). The resulting voltammogram suggests that the first oxidation occurring at +0.5 V is reversible and reflective of the target compound **8**.

5. Future Directions

In the future, with a now established synthetic procedure to produce complex **6**, well defined crystals suitable for structural analysis will be obtained. Additionally, its chemical and electrochemical oxidation may be studied. Further exploration of the electrochemistry of **8** will be performed, allowing for a better understanding of the stability of this compound upon oxidation. Further computational studies will be performed in attempt to rationalize the unexpected formation of **9** and doubly oxidized iminobenzosemiquinone **11** from **8**. Finally, **8** will be further reacted with other mild oxidizing agents such as dichloride and diphenyl disulfide to further assess its redox properties.

6. References

- (1) Anastas, P.; Eghbali, N. Green Chemistry: Principles and Practice. *Chem Soc Rev* **2010**, *39* (1), 301–312. <https://doi.org/10.1039/B918763B>.
- (2) Sheldon, R. A. The E Factor 25 Years on: The Rise of Green Chemistry and Sustainability. *Green Chem.* **2017**, *19* (1), 18–43. <https://doi.org/10.1039/C6GC02157C>.
- (3) Ivanković, A.; Dronjić, A.; Bevanda, A.; Talić, S. Review of 12 Principles of Green Chemistry in Practice. *Int. J. Sustain. Green Energy* **2017**, *6*, 39–48. <https://doi.org/10.11648/j.ijrse.20170603.12>.
- (4) Poliakoff, M.; Fitzpatrick, J. M.; Farren, T. R.; Anastas, P. T. Green Chemistry: Science and Politics of Change. *Science* **2002**, *297* (5582), 807–810. <https://doi.org/10.1126/science.297.5582.807>.
- (5) Cue, B. W.; Zhang, J. Green Process Chemistry in the Pharmaceutical Industry. *Green Chem. Lett. Rev.* **2009**, *2* (4), 193–211. <https://doi.org/10.1080/17518250903258150>.
- (6) Anastas, P. T.; Kirchhoff, M. M.; Williamson, T. C. Catalysis as a Foundational Pillar of Green Chemistry. *Appl. Catal. Gen.* **2001**, *221* (1–2), 3–13. [https://doi.org/10.1016/S0926-860X\(01\)00793-1](https://doi.org/10.1016/S0926-860X(01)00793-1).
- (7) Luo, J.; G. Oliver, A.; McIndoe, J. S. A Detailed Kinetic Analysis of Rhodium-Catalyzed Alkyne Hydrogenation. *Dalton Trans.* **2013**, *42* (31), 11312–11318. <https://doi.org/10.1039/C3DT51212F>.
- (8) Rosenberg, L.; Davis, C. W.; Yao, J. Catalytic Dehydrogenative Coupling of Secondary Silanes Using Wilkinson's Catalyst. *J. Am. Chem. Soc.* **2001**, *123* (21), 5120–5121. <https://doi.org/10.1021/ja015697i>.

- (9) Ludwig, J. R.; Schindler, C. S. Catalyst: Sustainable Catalysis. *Chem* **2017**, *2* (3), 313–316. <https://doi.org/10.1016/j.chempr.2017.02.014>.
- (10) Eisenberg, R.; Gray, H. B. Noninnocence in Metal Complexes: A Dithiolene Dawn. *Inorg. Chem.* **2011**, *50* (20), 9741–9751. <https://doi.org/10.1021/ic2011748>.
- (11) Schneider, U.; Kobayashi, S. Low-Oxidation State Indium-Catalyzed C–C Bond Formation. *Acc. Chem. Res.* **2012**, *45* (8), 1331–1344. <https://doi.org/10.1021/ar300008t>.
- (12) Alfonsi, K.; Colberg, J.; Dunn, P. J.; Fevig, T.; Jennings, S.; Johnson, T. A.; Kleine, H. P.; Knight, C.; Nagy, M. A.; Perry, D. A.; Stefaniak, M. Green Chemistry Tools to Influence a Medicinal Chemistry and Research Chemistry Based Organisation. *Green Chem* **2008**, *10* (1), 31–36. <https://doi.org/10.1039/B711717E>.
- (13) Alfantazi, A. M.; Moskalyk, R. R. Processing of Indium: A Review. *Miner. Eng.* **2003**, *16* (8), 687–694. [https://doi.org/10.1016/S0892-6875\(03\)00168-7](https://doi.org/10.1016/S0892-6875(03)00168-7).
- (14) Green, M. *Organometallic Chemistry*; Royal Society of Chemistry, 2002.
- (15) Lyaskovskyy, V.; de Bruin, B. Redox Non-Innocent Ligands: Versatile New Tools to Control Catalytic Reactions. *ACS Catal.* **2012**, *2* (2), 270–279. <https://doi.org/10.1021/cs200660v>.
- (16) Praneeth, V. K. K.; Ringenberg, M. R.; Ward, T. R. Redox-Active Ligands in Catalysis. *Angew. Chem. Int. Ed.* **2012**, *51* (41), 10228–10234. <https://doi.org/10.1002/anie.201204100>.
- (17) Lyaskovskyy, V.; de Bruin, B. Redox Non-Innocent Ligands: Versatile New Tools to Control Catalytic Reactions. *ACS Catal.* **2012**, *2* (2), 270–279. <https://doi.org/10.1021/cs200660v>.

- (18) Piskunov, A. V.; Mescheryakova, I. N.; Fukin, G. K.; Baranov, E. V.; Hummert, M.; Shavyrin, A. S.; Cherkasov, V. K.; Abakumov, G. A. Oxidation by Oxygen and Sulfur of Tin(IV) Derivatives Containing a Redox-Active *o*-Amidophenolate Ligand. *Chem. - Eur. J.* **2008**, *14* (32), 10085–10093. <https://doi.org/10.1002/chem.200801203>.
- (19) Singh, K.; Kundu, A.; Adhikari, D. Ligand-Based Redox: Catalytic Applications and Mechanistic Aspects. *ACS Catal.* **2022**, *12* (20), 13075–13107. <https://doi.org/10.1021/acscatal.2c02655>.
- (20) Singh, B.; Indra, A. Role of Redox Active and Redox Non-Innocent Ligands in Water Splitting. *Inorganica Chim. Acta* **2020**, *506*, 119440. <https://doi.org/10.1016/j.ica.2020.119440>.
- (21) Lyaskovskyy, V.; de Bruin, B. Redox Non-Innocent Ligands: Versatile New Tools to Control Catalytic Reactions. *ACS Catal.* **2012**, *2* (2), 270–279. <https://doi.org/10.1021/cs200660v>.
- (22) Sproules, S.; Wieghardt, K. O-Dithiolene and o-Aminothiolate Chemistry of Iron: Synthesis, Structure and Reactivity. *Coord. Chem. Rev.* **2010**, *254* (13–14), 1358–1382. <https://doi.org/10.1016/j.ccr.2009.12.012>.
- (23) Luca, O. R.; Crabtree, R. H. Redox-Active Ligands in Catalysis. *Chem Soc Rev* **2013**, *42* (4), 1440–1459. <https://doi.org/10.1039/C2CS35228A>.
- (24) Amijs, C. H. M.; van Klink, G. P. M.; van Koten, G. Carbon Tetrachloride Free Benzylic Brominations of Methyl Aryl Halides. *Green Chem.* **2003**, *5* (4), 470. <https://doi.org/10.1039/b304673g>.
- (25) Schumann, H.; Hartmann, U.; Wassermann, W. Synthesis and Characterization of Organogallium and Organoindium Compounds with Tridentate 2,6-

- Bis[(Dialkylamino)Methyl]Phenyl Ligands. *Chem. Ber.* **1991**, *124* (7), 1567–1569.
<https://doi.org/10.1002/cber.19911240714>.
- (26) Ringenberg, M. R.; Nilges, M. J.; Rauchfuss, T. B.; Wilson, S. R. Oxidation of Dihydrogen by Iridium Complexes of Redox-Active Ligands. *Organometallics* **2010**, *29* (8), 1956–1965. <https://doi.org/10.1021/om9010593>.
- (27) Blackmore, K. J.; Ziller, J. W.; Heyduk, A. F. “Oxidative Addition” to a Zirconium(IV) Redox-Active Ligand Complex. *Inorg. Chem.* **2005**, *44* (16), 5559–5561.
<https://doi.org/10.1021/ic050997c>.
- (28) Schumann, H.; Wassermann, W.; Dietrich, A. ChemInform Abstract: Synthesis and Molecular Structure of CH₃(2,6-((C₂H₅)₂NCH₂)₂C₆H₃)InCl, an Intramolecular Stabilized Monomeric Diorganoindium Chloride. *ChemInform* **1989**, *20* (38).
<https://doi.org/10.1002/chin.198938285>.
- (29) Ershova, I. V.; Bogomyakov, A. S.; Fukin, G. K.; Piskunov, A. V. Features of Magnetic Behavior in the Row of Pentacoordinated Bis- *o* -Iminobenzosemiquinonato Metal (Al, Ga, In) Complexes. *Eur. J. Inorg. Chem.* **2019**, *2019* (7), 938–948.
<https://doi.org/10.1002/ejic.201801348>.
- (30) Piskunov, A. V.; Meshcheryakova, I. N.; Ershova, I. V.; Bogomyakov, A. S.; Cherkasov, A. V.; Fukin, G. K. The Reactivity of O-Amidophenolate Indium(III) Complexes towards Different Oxidants. *RSC Adv* **2014**, *4* (80), 42494–42505.
<https://doi.org/10.1039/C4RA05408C>.
- (31) Gaussian16, RevisionC.01, M. J. Frisch, G. W. Trucks, H. B. Schlegel, G. E. Scuseria, M. A. Robb, J. R. Cheeseman, G. Scalmani, V. Barone, G. A. Petersson, H. Nakatsuji, X. Li, M. Caricato, A. V. Marenich, J. Bloino, B. G. Janesko, R. Gomperts, B. Mennucci, H. P.

Hratchian, J. V. Ortiz, A. F. Izmaylov, J. L. Sonnenberg, D. Williams-Young, F. Ding, F. Lipparini, F. Egidi, J. Goings, B. Peng, A. Petrone, T. Henderson, D. Ranasinghe, V. G. Zakrzewski, J. Gao, N. Rega, G. Zheng, W. Liang, M. Hada, M. Ehara, K. Toyota, R. Fukuda, J. Hasegawa, M. Ishida, T. Nakajima, Y. Honda, O. Kitao, H. Nakai, T. Vreven, K. Throssell, J. A. Montgomery, Jr., J. E. Peralta, F. Ogliaro, M. J. Bearpark, J. J. Heyd, E. N. Brothers, K. N. Kudin, V. N. Staroverov, T. A. Keith, R. Kobayashi, J. Normand, K. Raghavachari, A. P. Rendell, J. C. Burant, S. S. Iyengar, J. Tomasi, M. Cossi, J. M. Millam, M. Klene, C. Adamo, R. Cammi, J. W. Ochterski, R. L. Martin, K. Morokuma, O. Farkas, J. B. Foresman, and D. J. Fox, Gaussian, Inc., Wallingford CT, 2016.

7. Appendix

Appendix A: Spectroscopic data

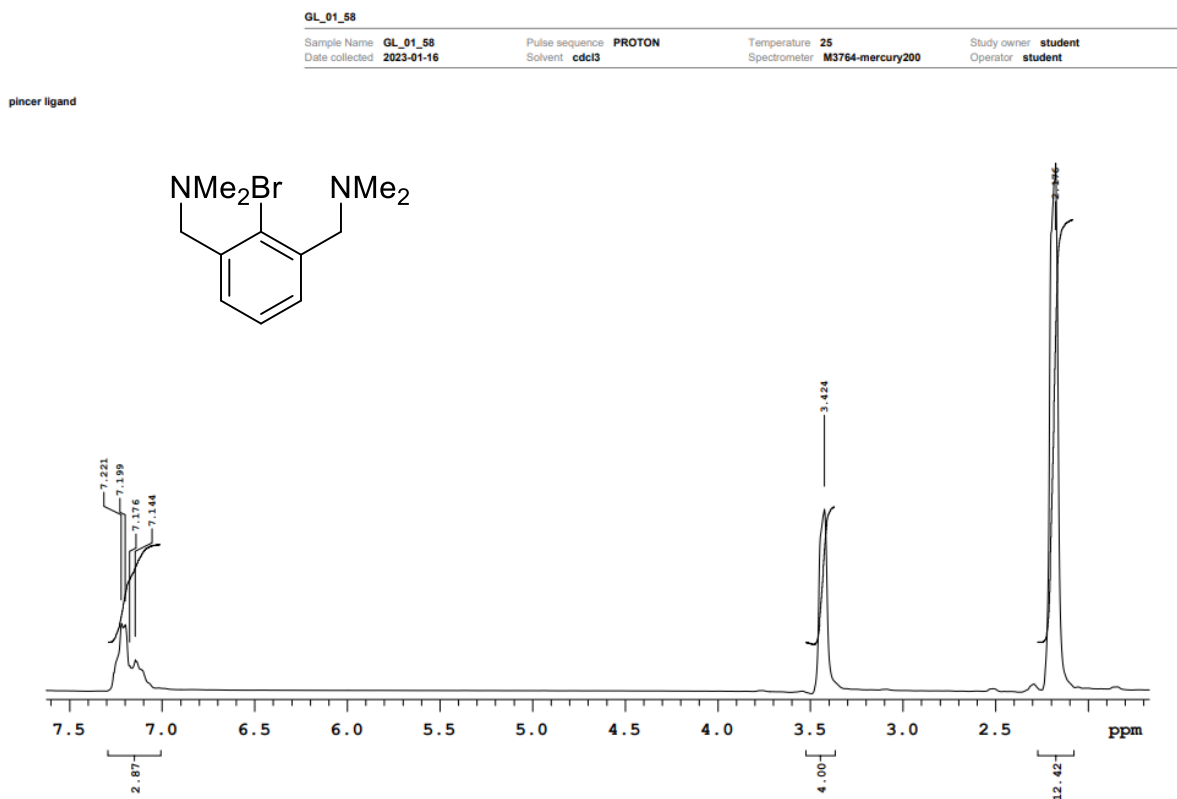


Figure A.1: ¹H NMR spectrum of (NCN)Br (**1**) in CDCl₃.

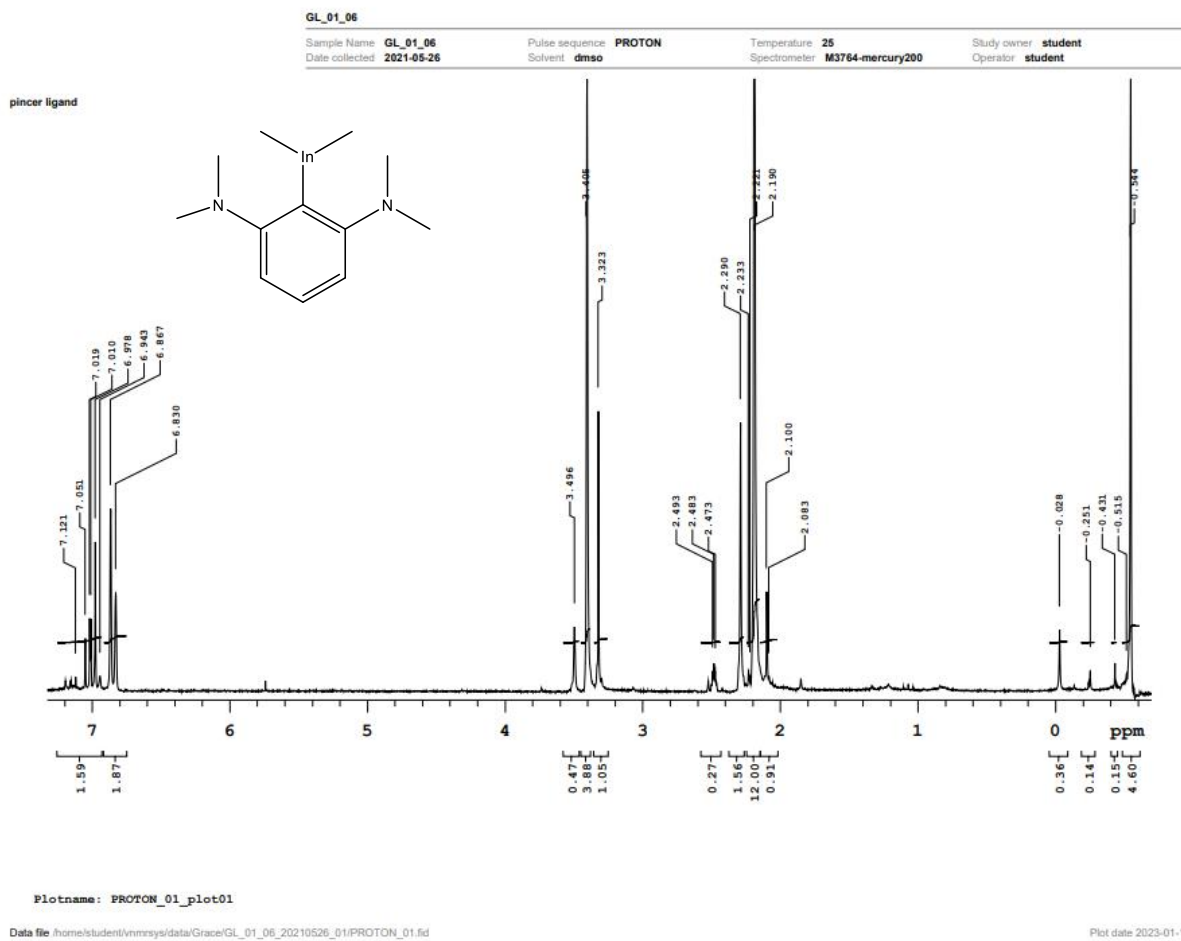


Figure A.2: ¹H NMR spectrum of NCNInMe₂ (2) in DMSO.

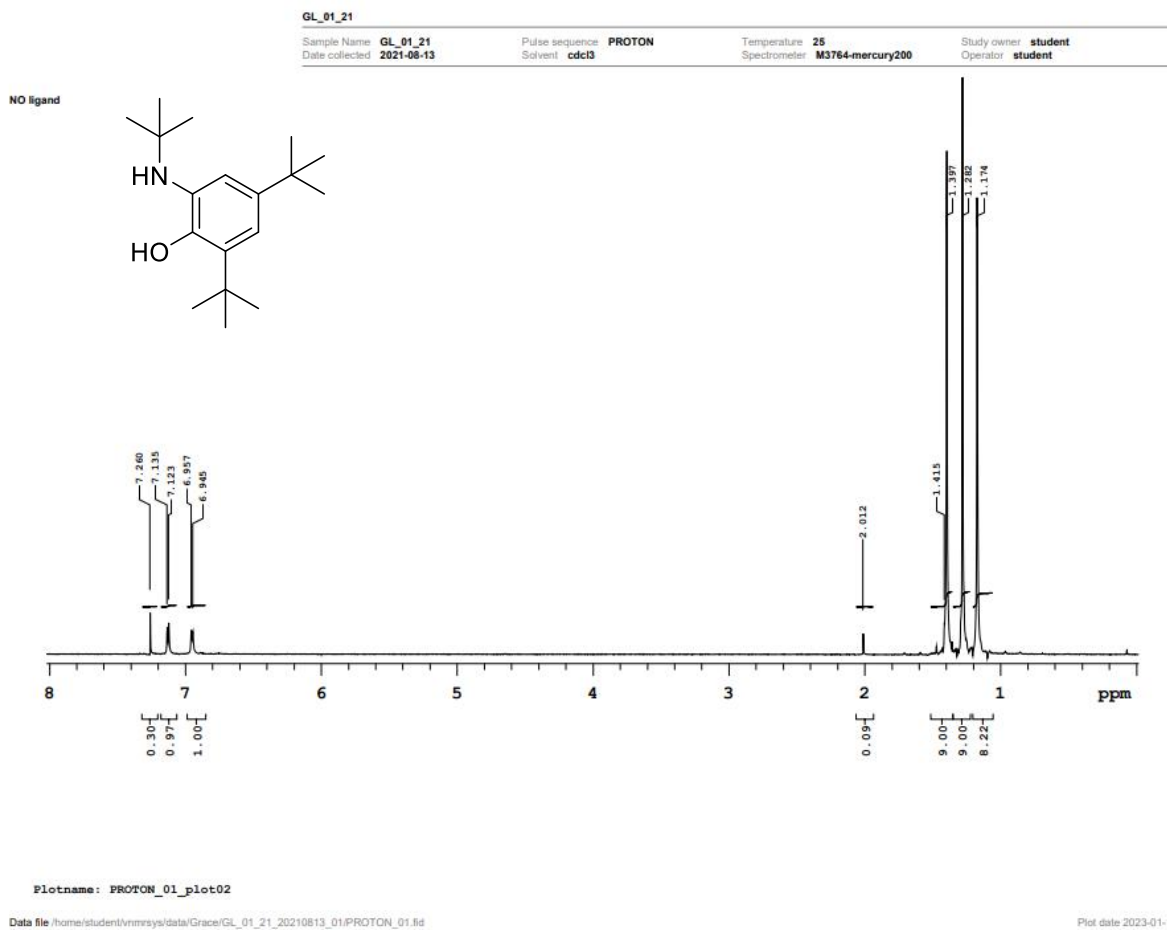


Figure A.3: ^1H NMR spectrum of $\text{H}_2(\text{NO})$ (**3**) in CDCl_3 .

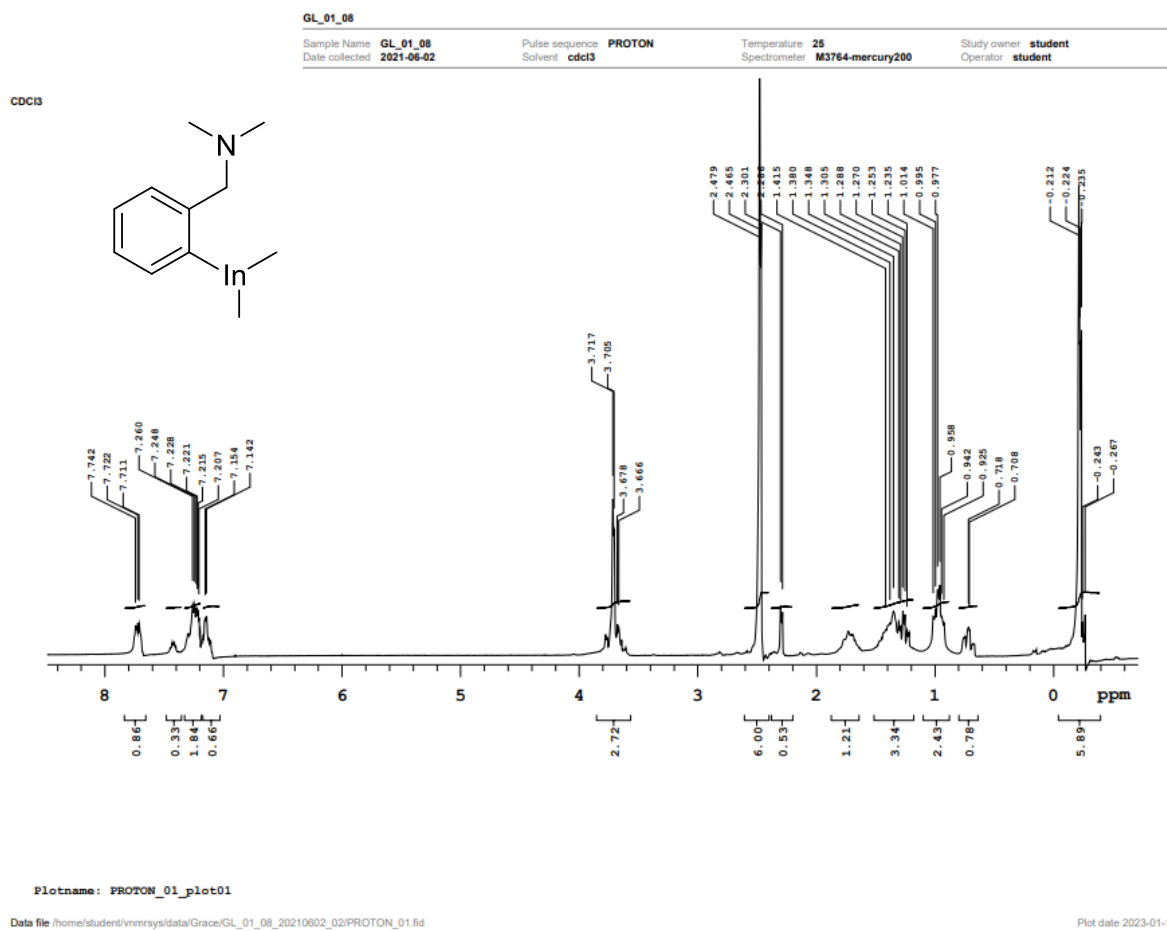


Figure A.4: ^1H NMR spectrum of (NC)InMe₂ (**4**) in CDCl₃.

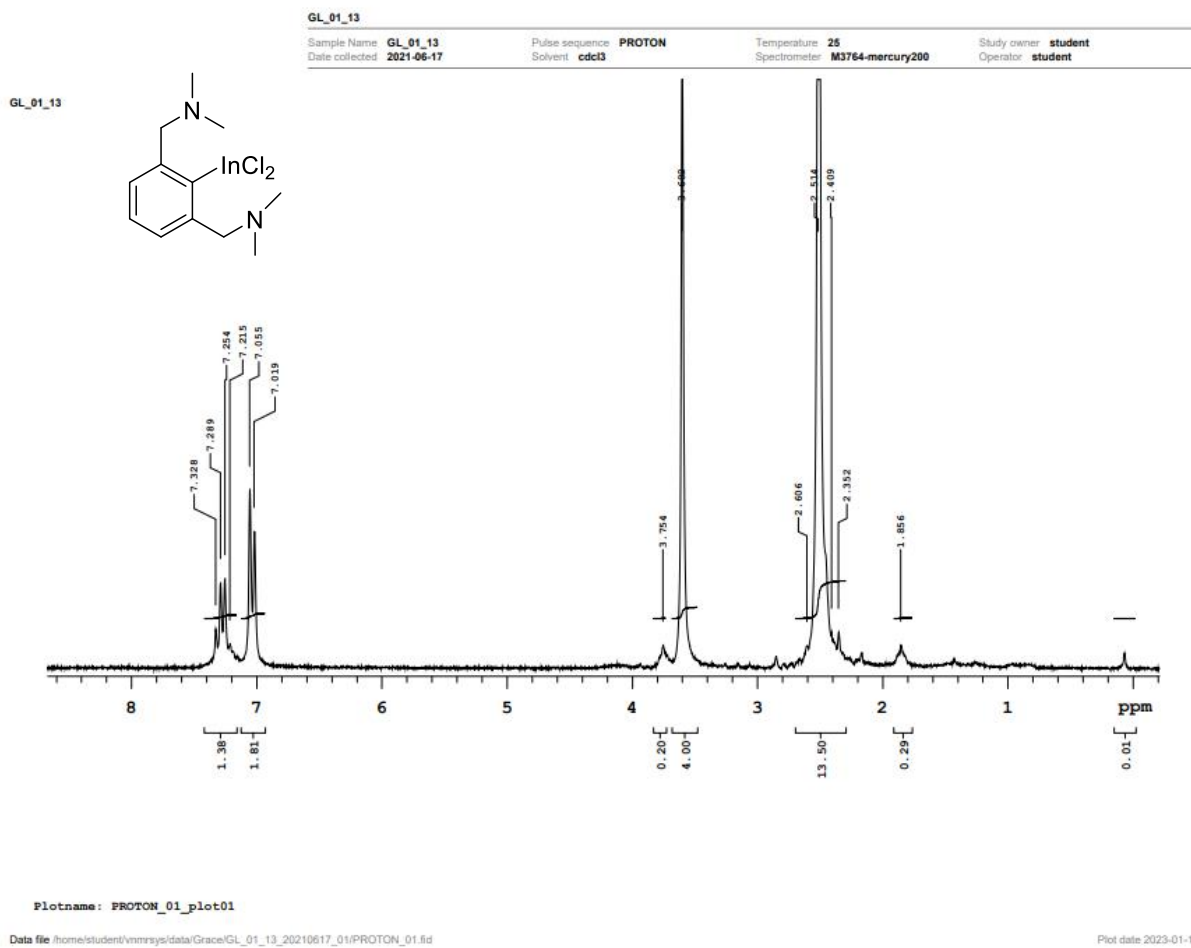


Figure A.5: ^1H NMR spectrum of (NCN)InCl₂ (**5**) in CDCl₃.

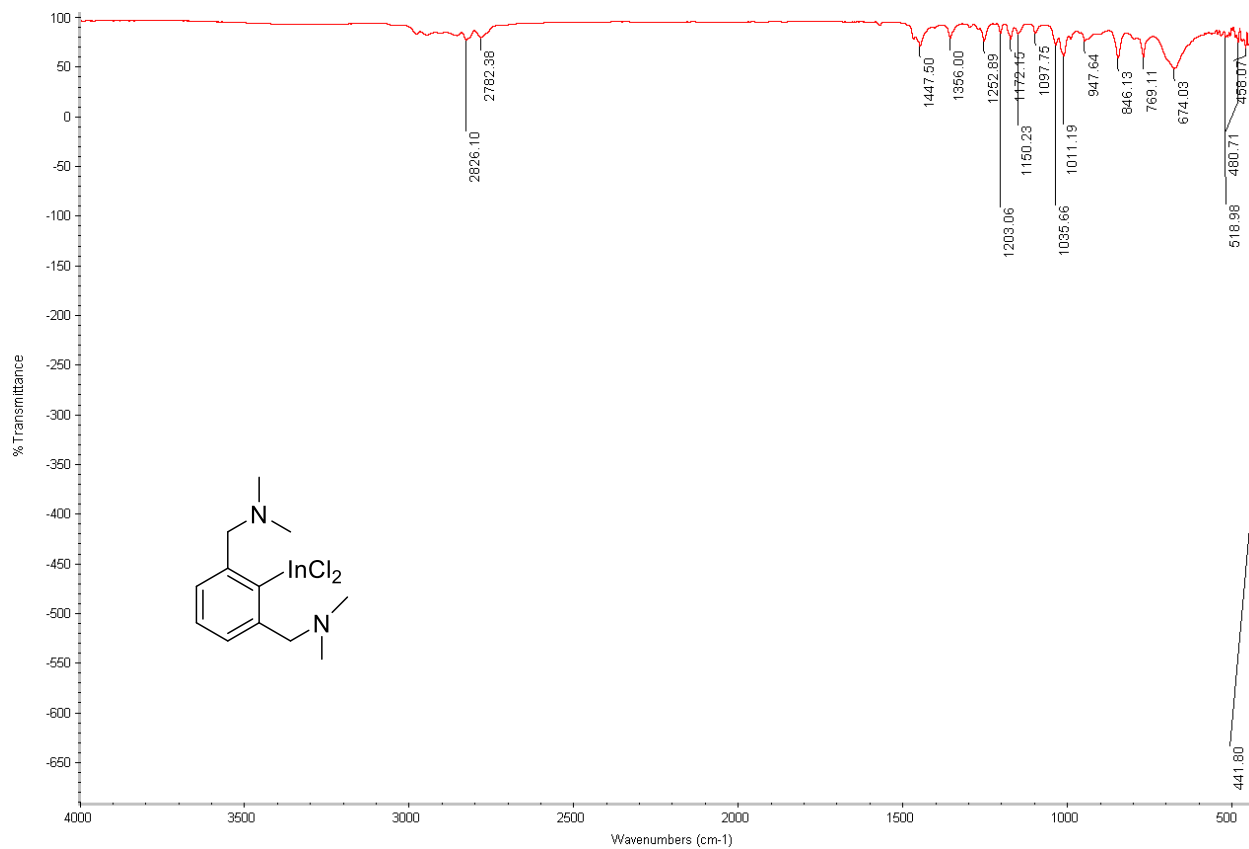


Figure A.6: FT-IR spectrum on (NCN)InCl₂ (5).

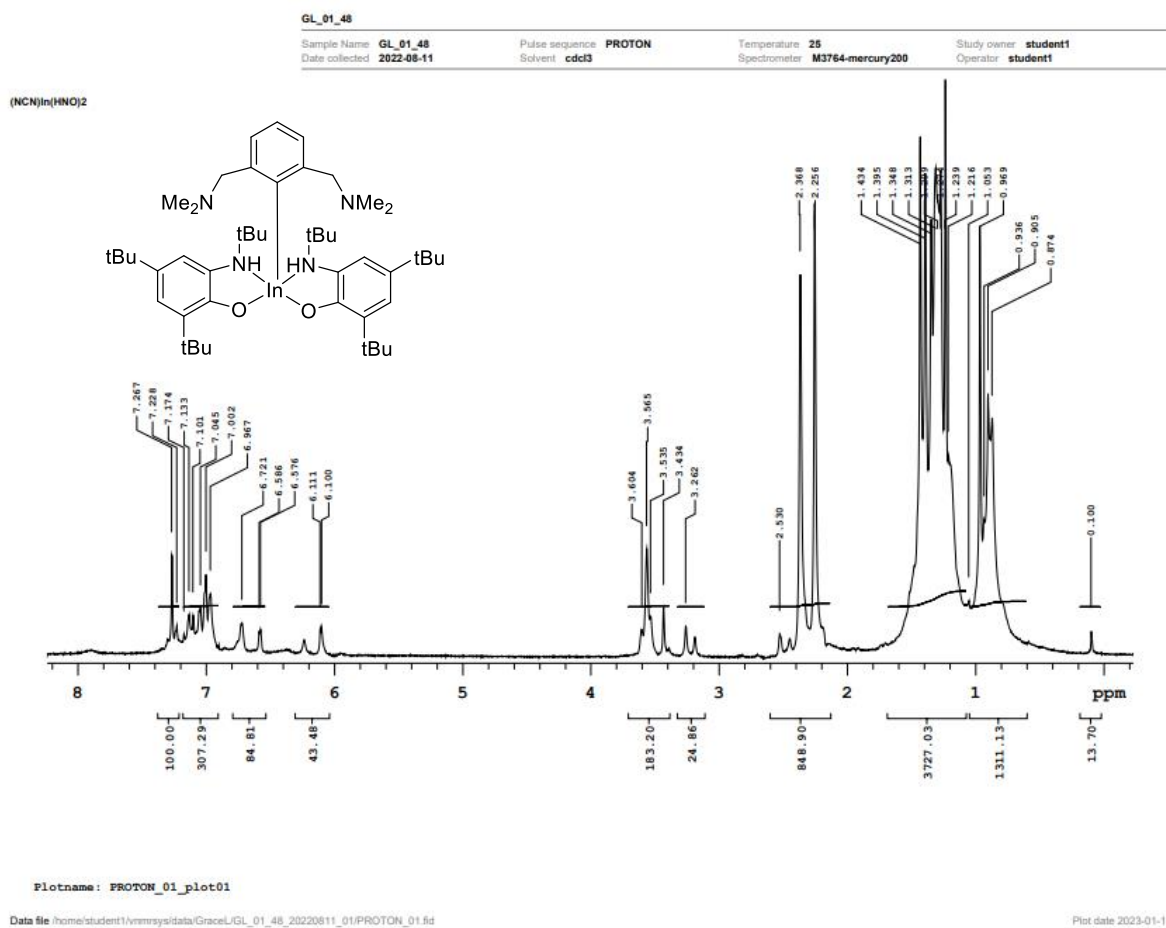


Figure A.7: ¹H NMR spectrum of (NCN)In(HNO)₂ (**6**) in CDCl₃.

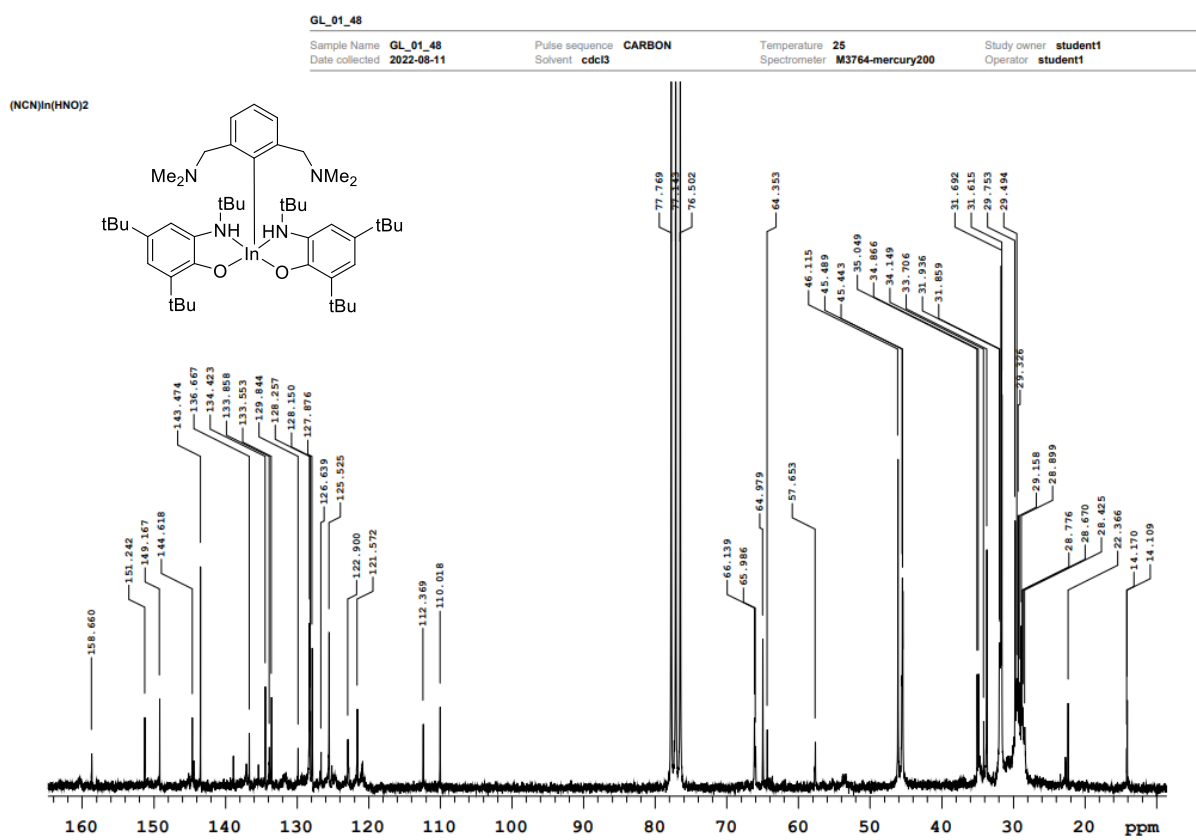


Figure A.8: $^{13}\text{C}\{^1\text{H}\}$ NMR spectrum of (NCN)In(HNO)₂ (6) in CDCl₃.

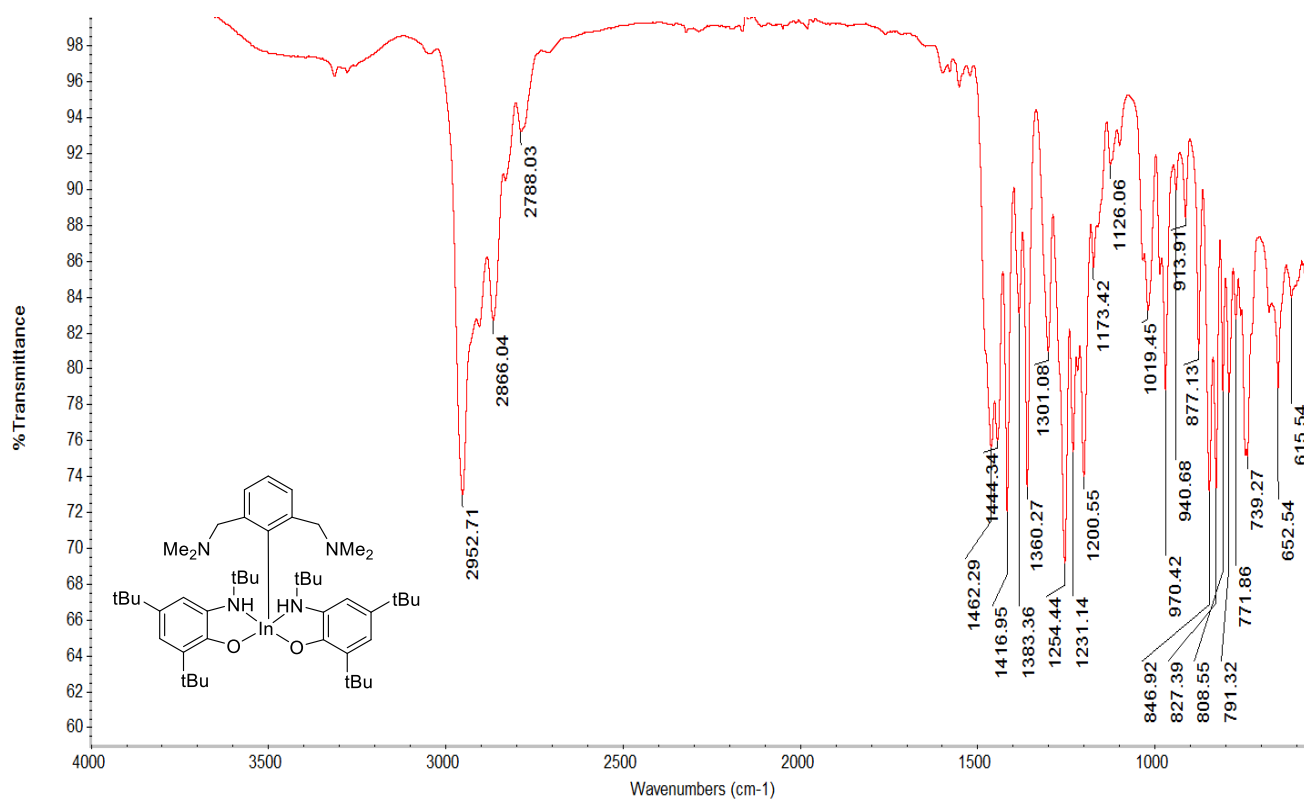


Figure A.9: FT-IR spectrum of (NCN)In(HNO)₂ (**6**).

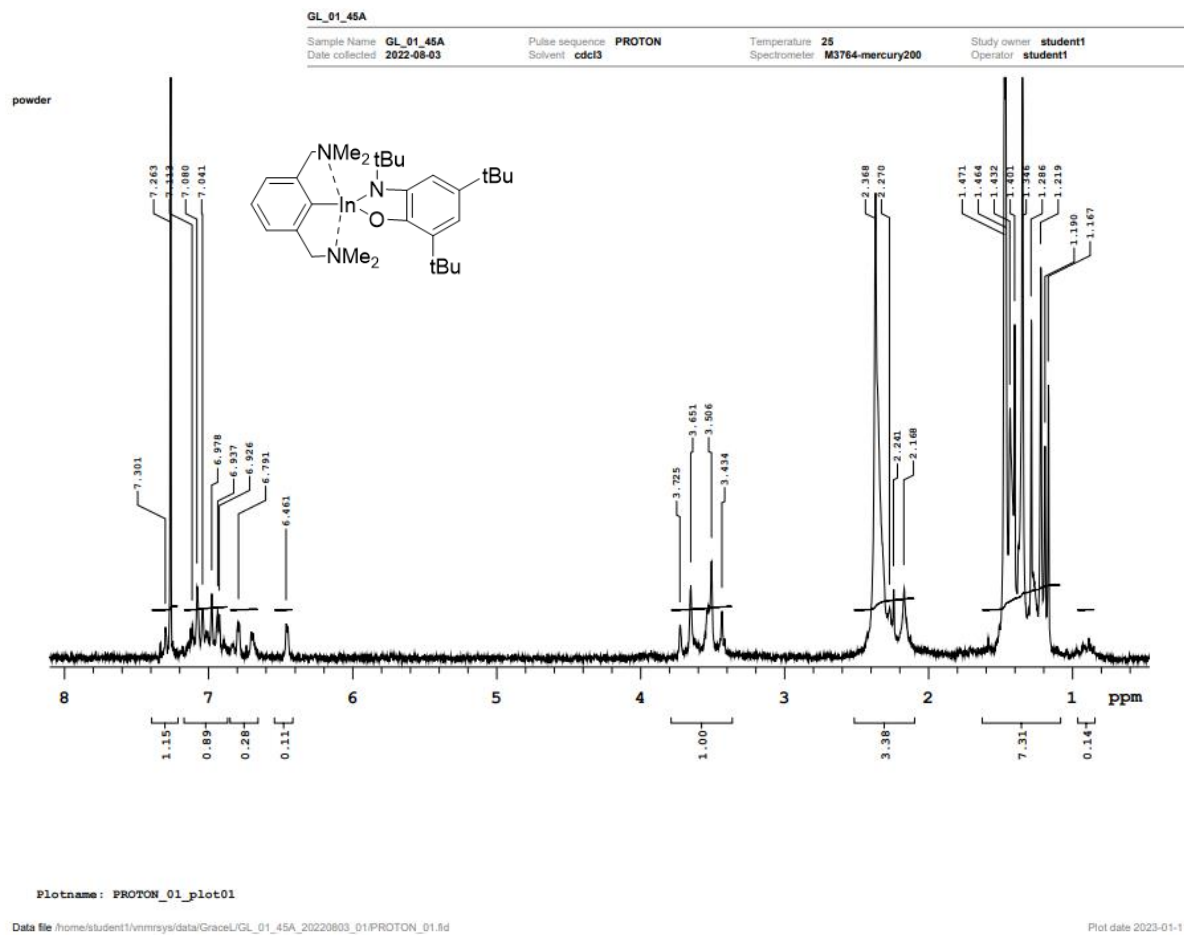


Figure A.10: ^1H NMR spectrum of (NCN)In(NO) (**7**) in CDCl_3 .

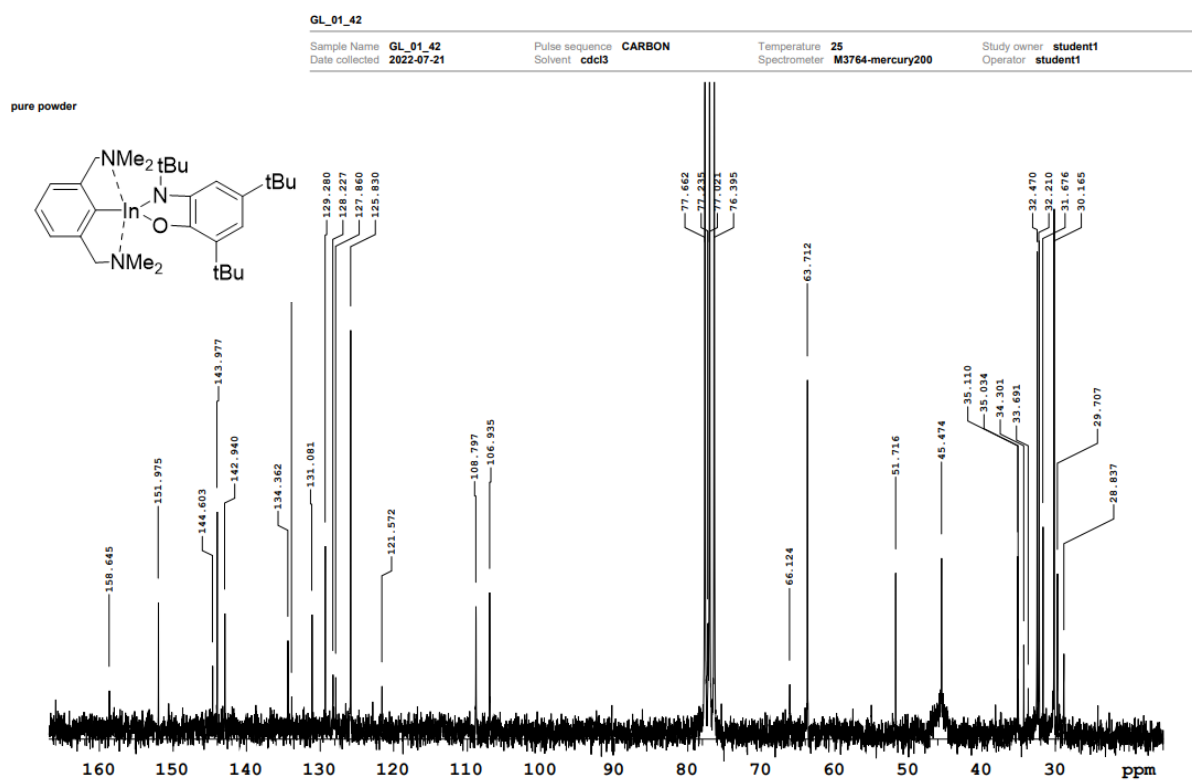


Figure A.11: $^{13}\text{C}\{^1\text{H}\}$ NMR spectrum of (NCN)In(NO) (**7**) in CDCl_3 .

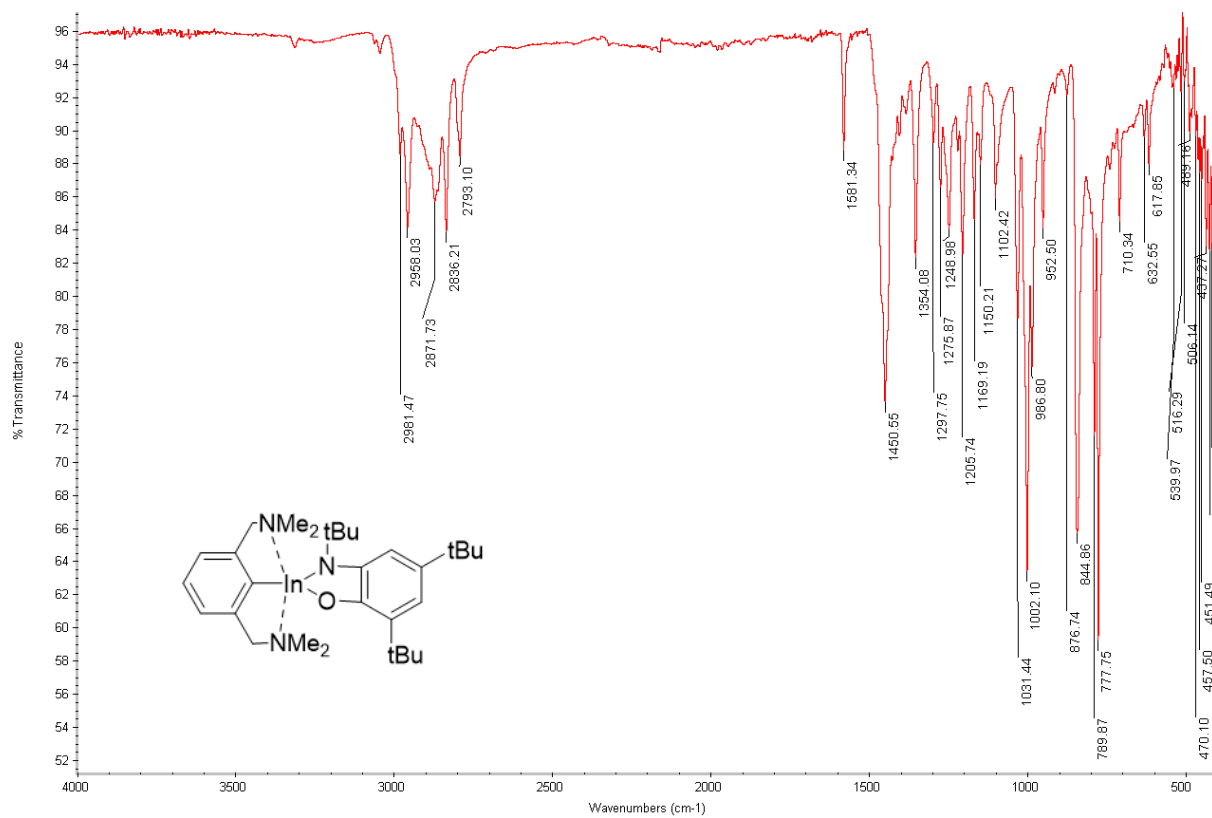


Figure A.12: FT-IR spectrum of (NCN)In(NO) (**7**).

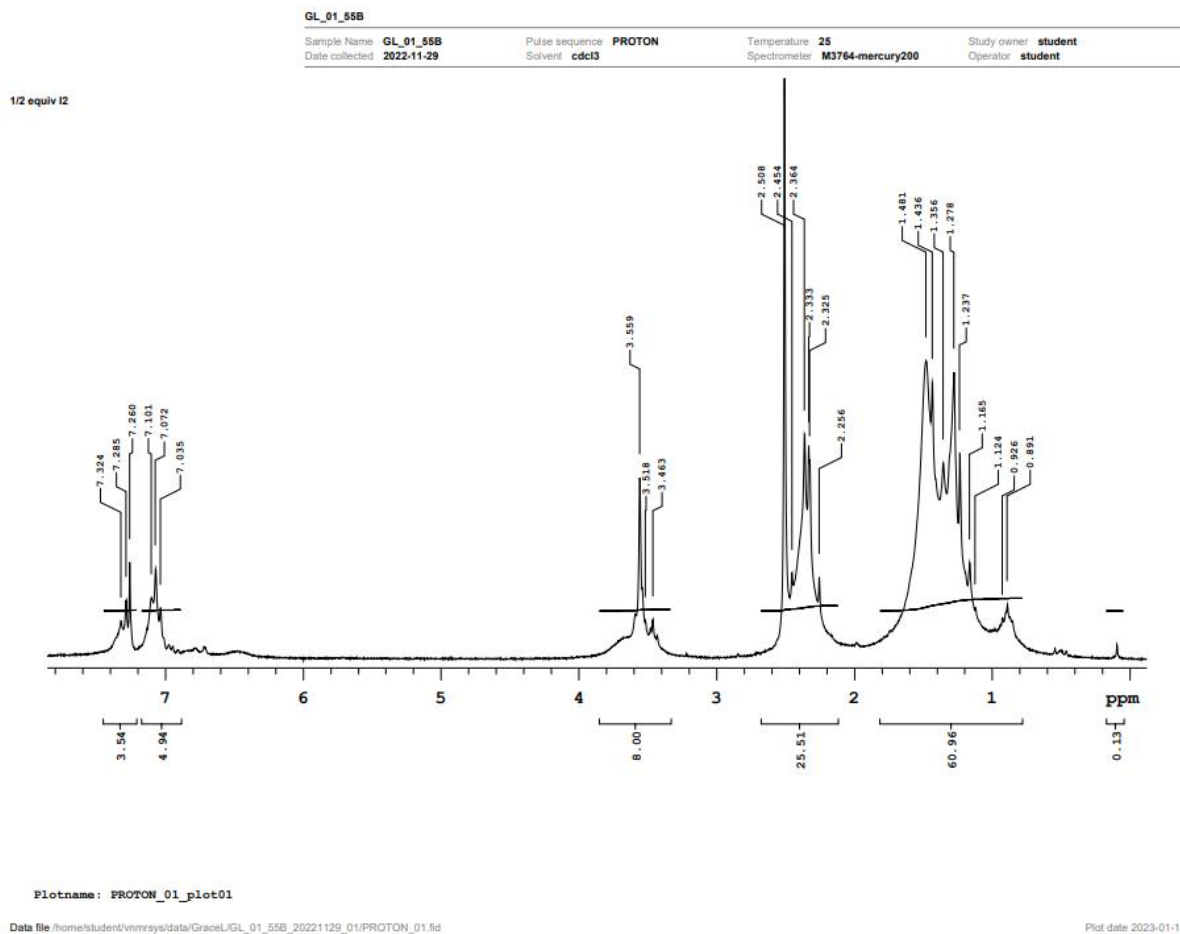


Figure A.13: ^1H NMR of $\frac{1}{2}$ equivalent of iodine (I_2) added to $(\text{NCN})\text{In}(\text{NO})$ (**8**) in CDCl_3 .

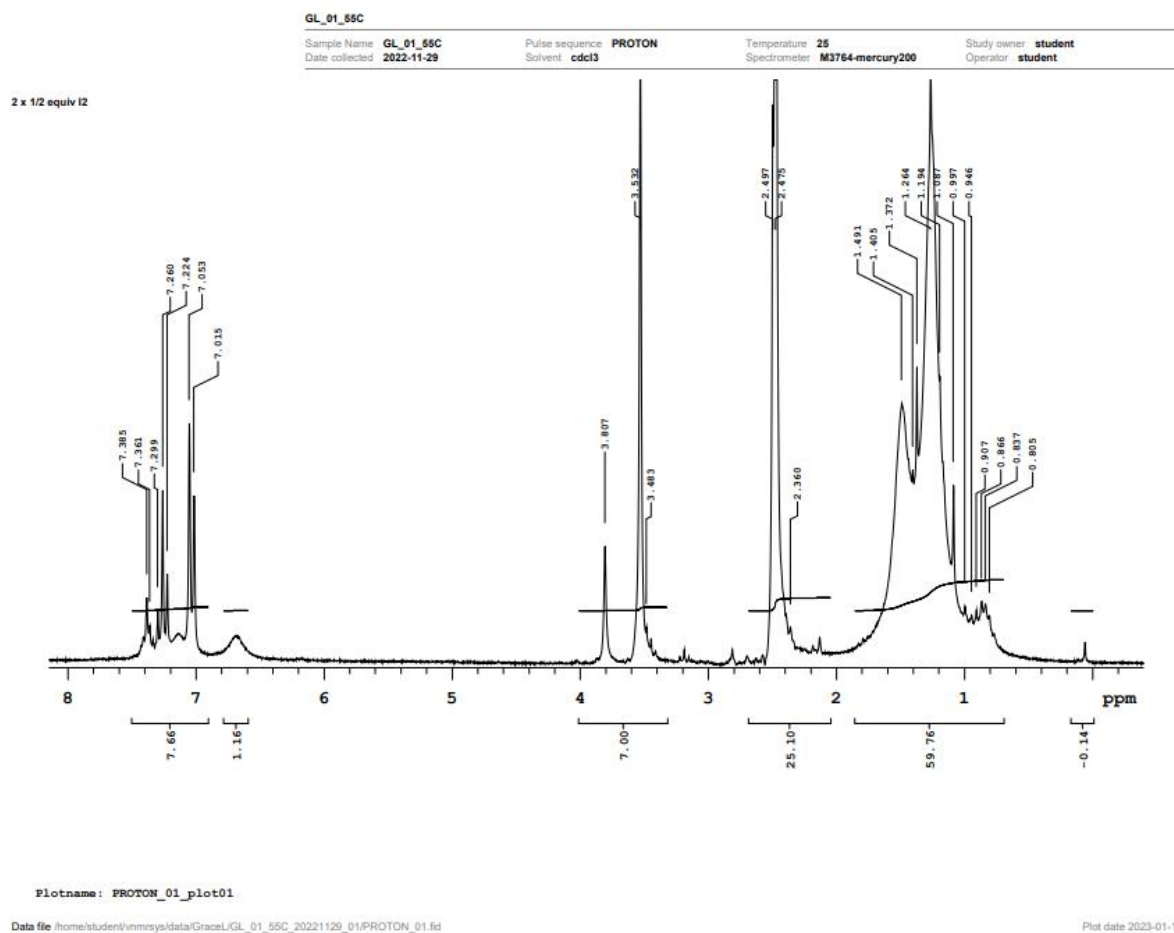


Figure A.14: ^1H NMR spectrum of 1 equivalent of Iodine added to $(\text{NCN})\text{In}(\text{NO})$ in CDCl_3 .

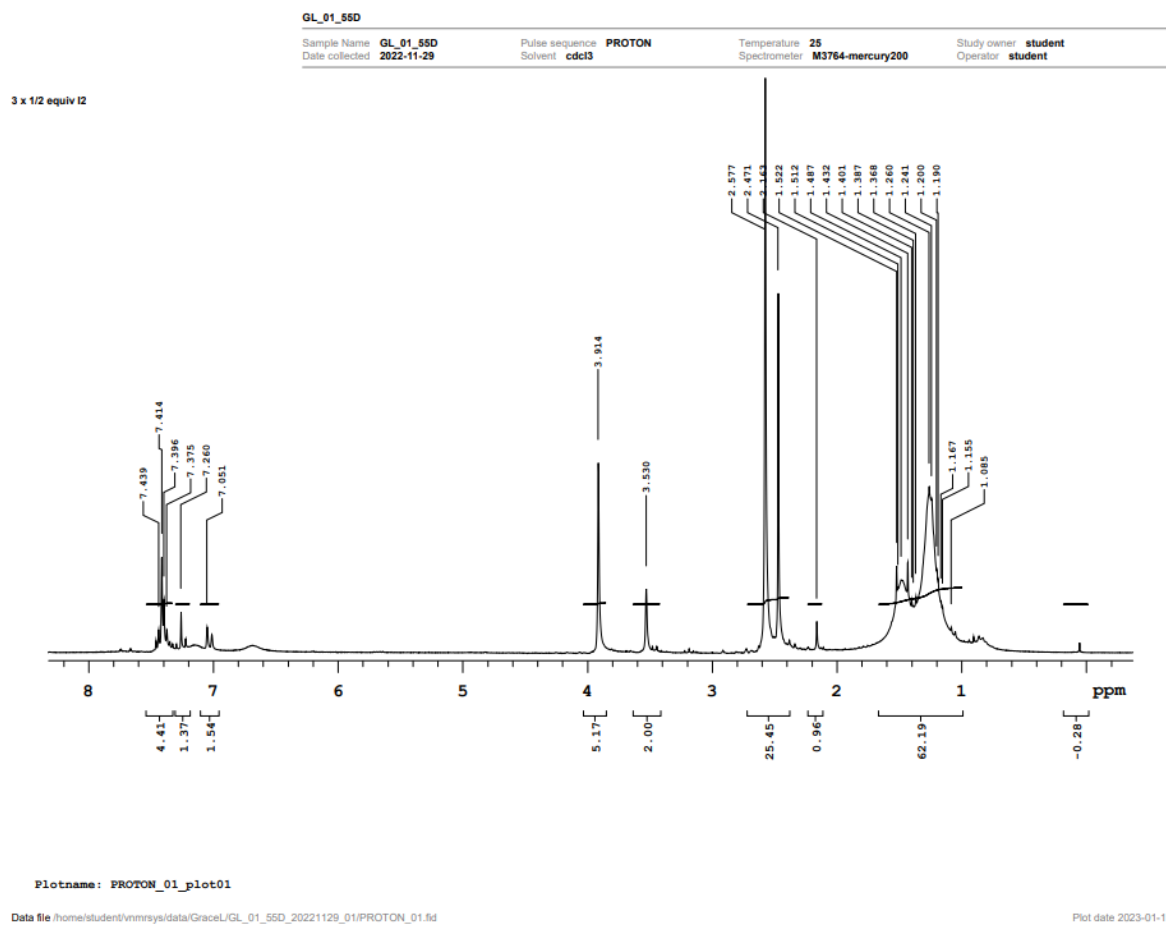


Figure A.15: ^1H NMR spectrum of 1 $\frac{1}{2}$ equivalents of iodine to $(\text{NCN})\text{In}(\text{NO})$ in CDCl_3 .

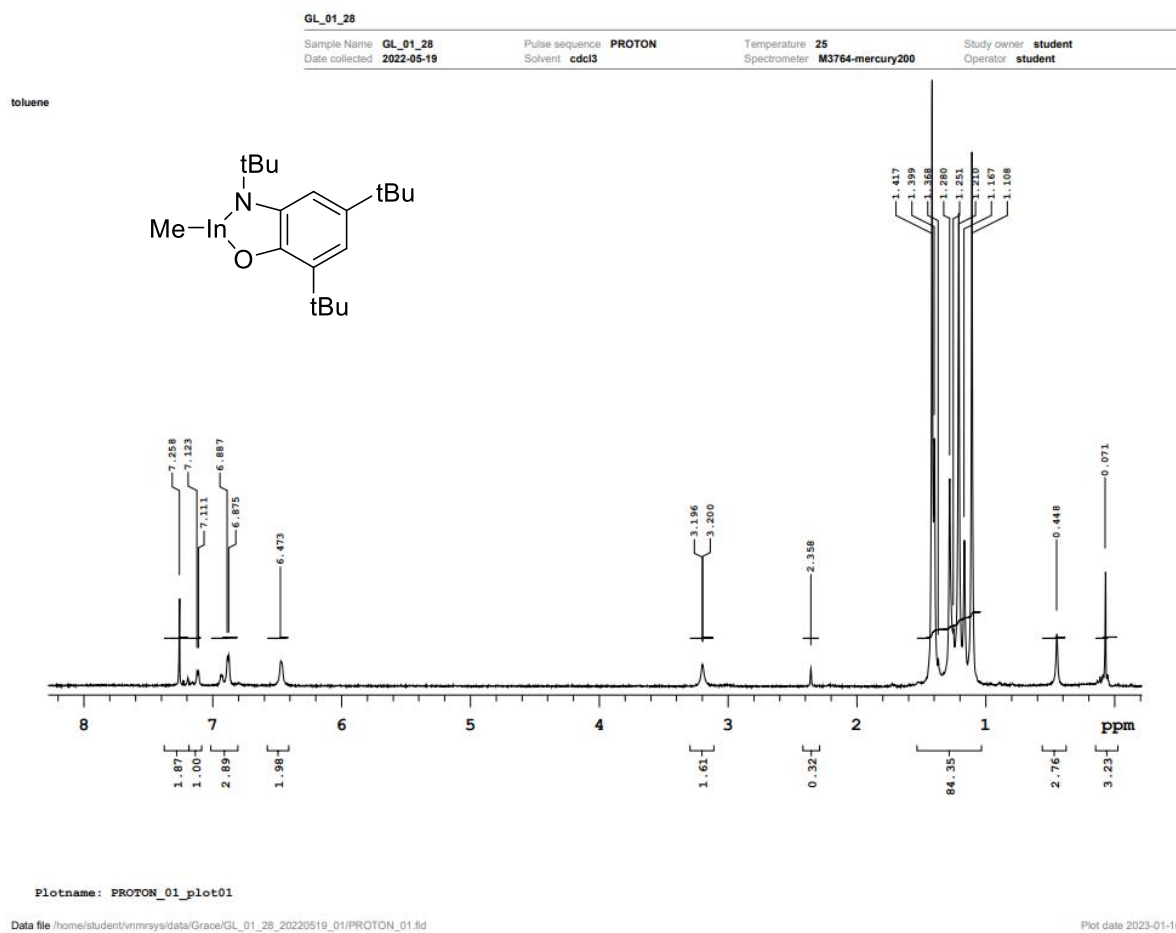


Figure A.16: ^1H NMR spectrum of (Me)In(NO) (**6**) in CDCl_3 .

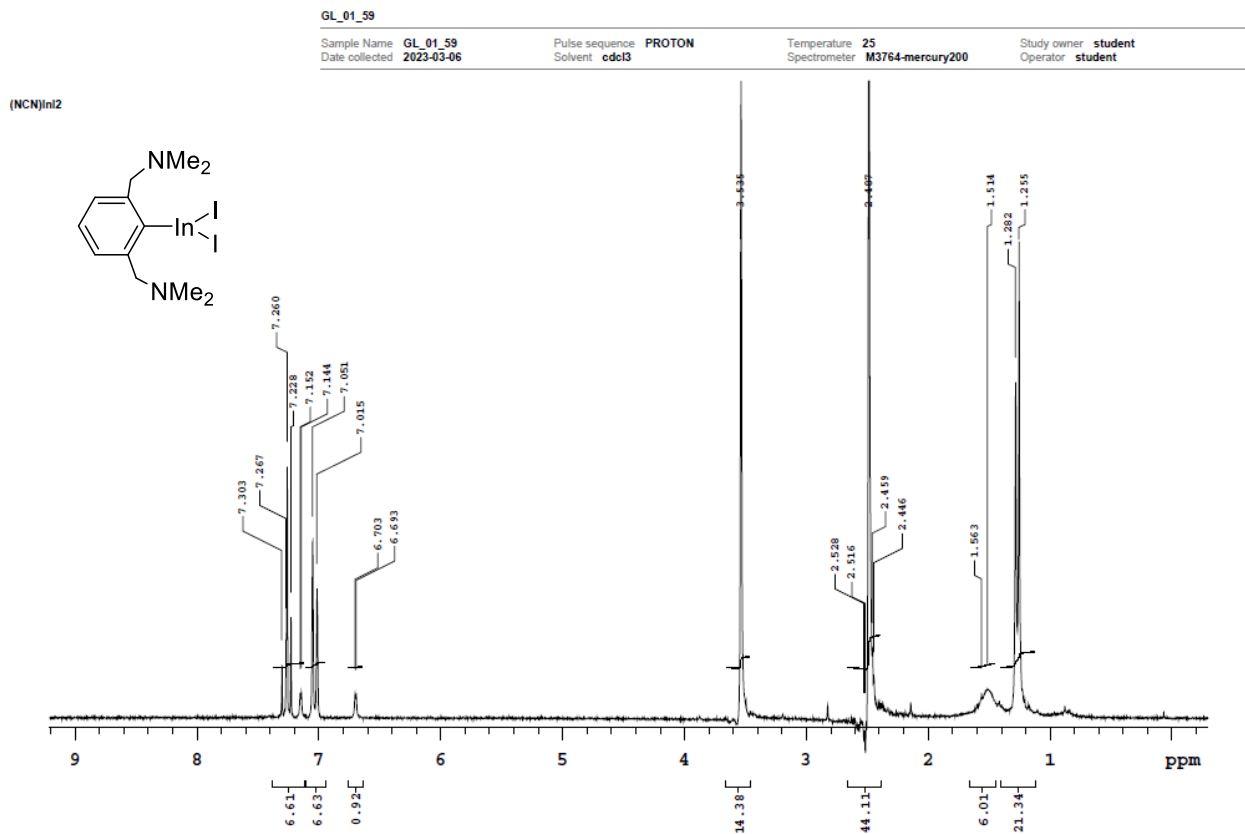


Figure A.17: ¹H NMR spectrum of (NCN)InI₂ (**9**) in CDCl₃.

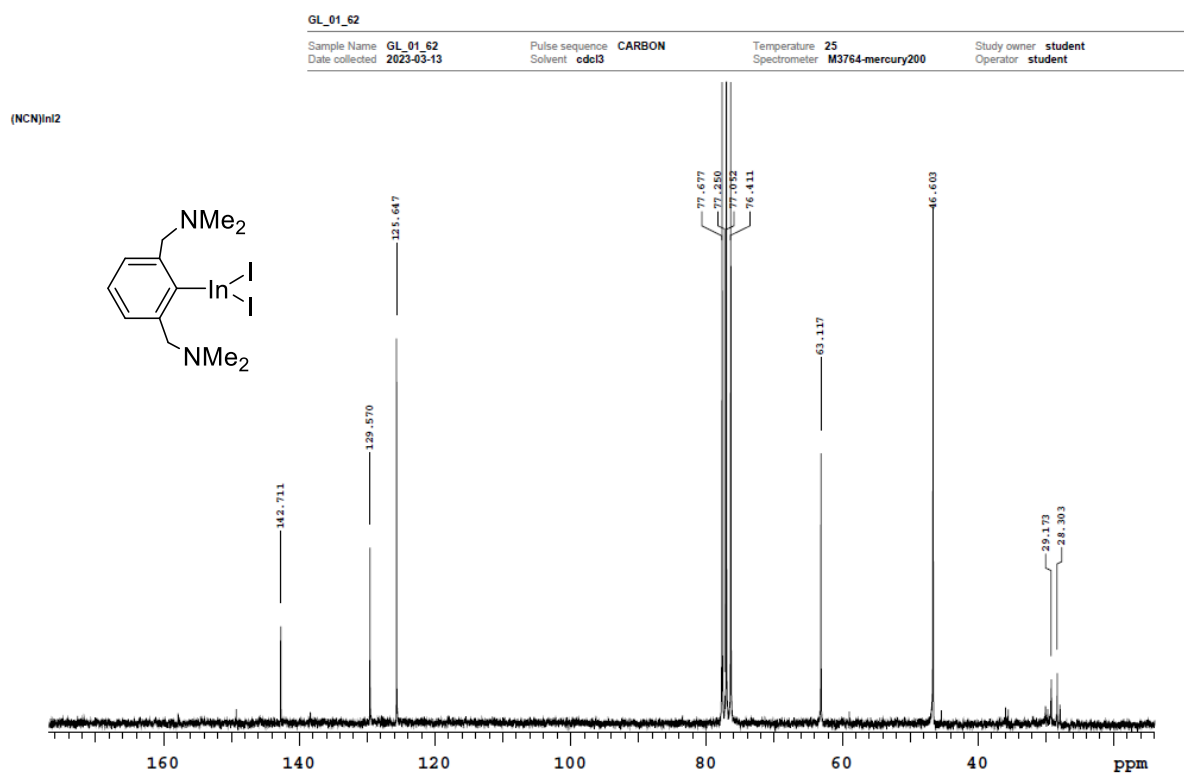


Figure A.18: $^{13}\text{C}\{^1\text{H}\}$ NMR spectrum of (NCN)InI₂ (**9**) in CDCl₃.

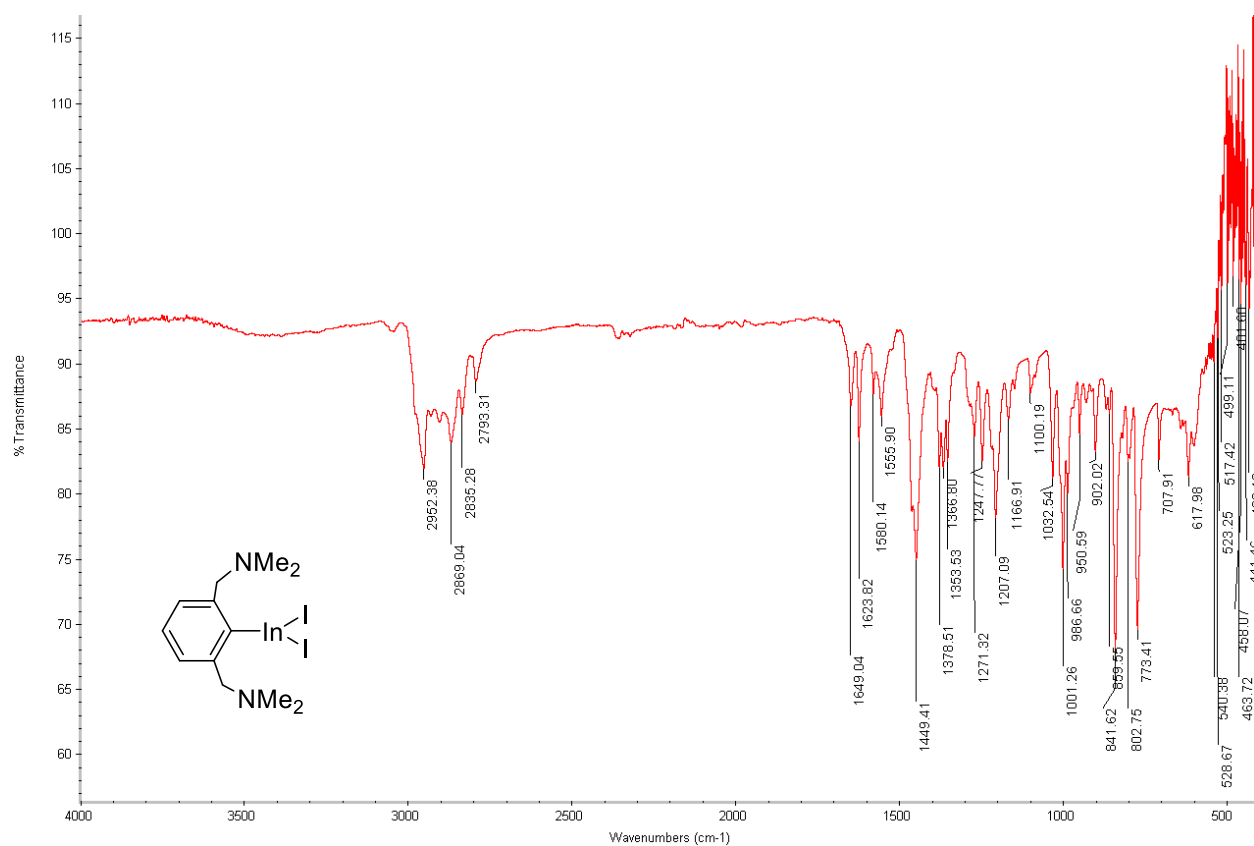


Figure A.19: FT-IR spectrum of (NCN)InI₂ (9).

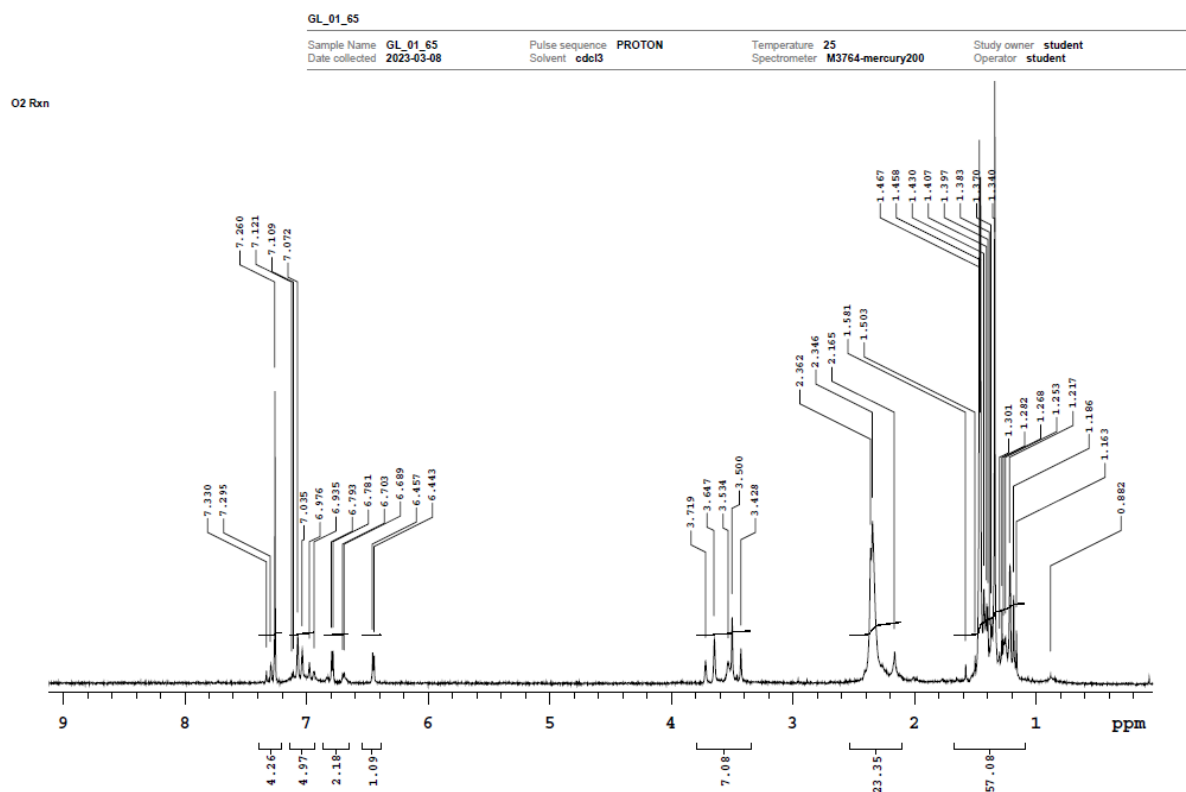


Figure A.20: ^1H NMR spectrum of reacting **8** with O_2 in CDCl_3 .

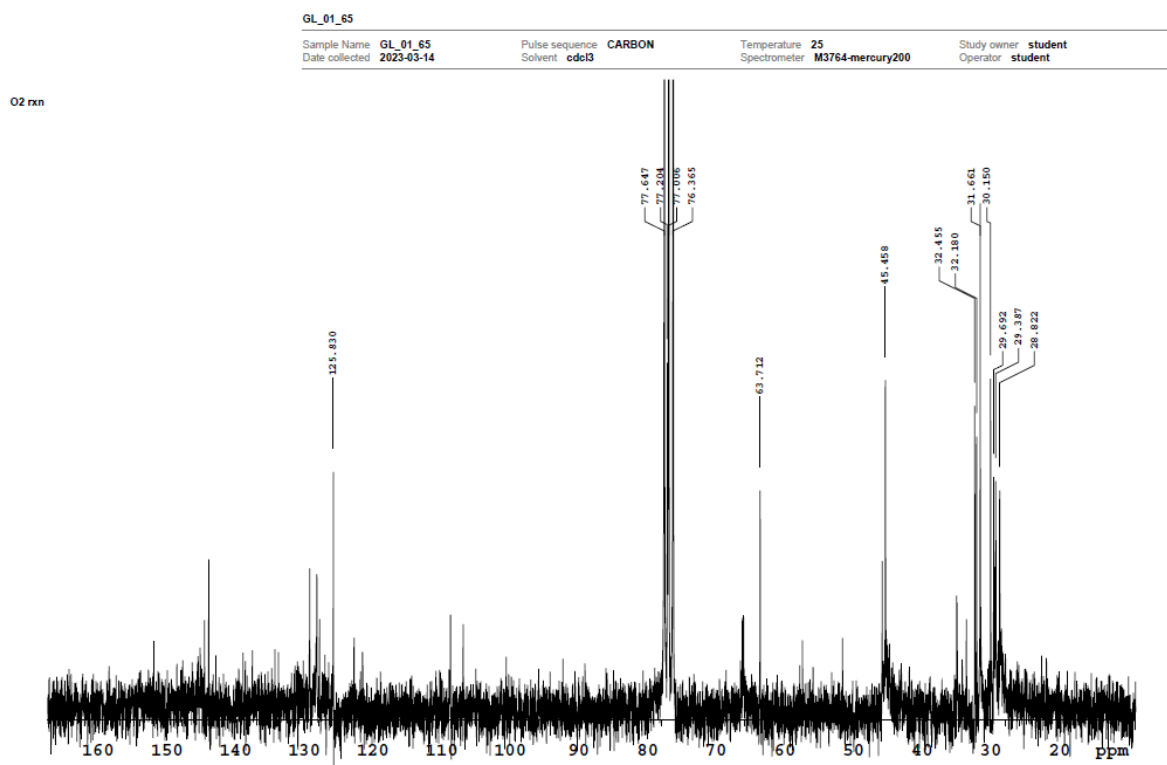


Figure A.21: $^{13}\text{C}\{^1\text{H}\}$ NMR spectrum of reacting **8** with O_2 in CDCl_3 .

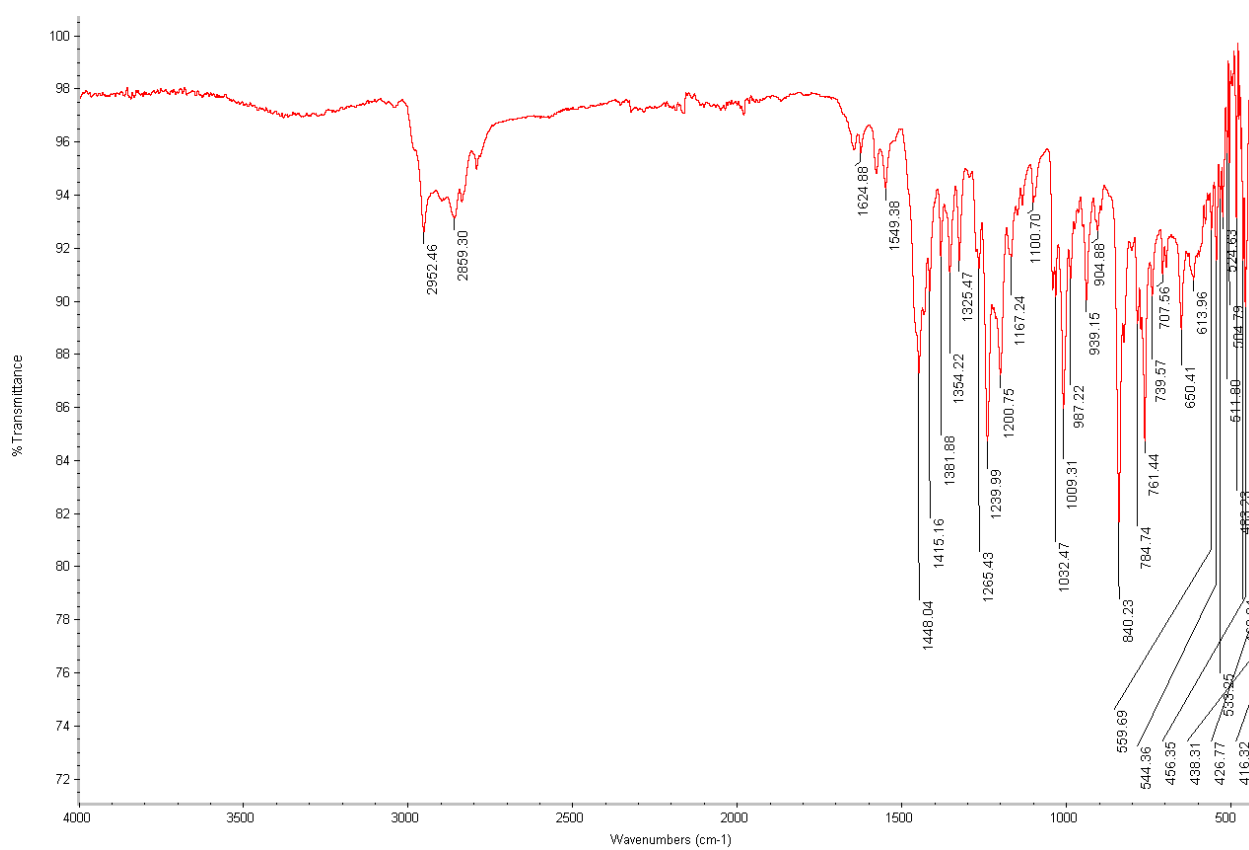


Figure A.22: FT-IR spectrum of reacting **8** with O₂.